University of Kerbala
College of Science
Chemistry Department

A GREEN SYNTHESIS OF COPPER OXIDE NANOPARTICLES AND STUDY THEIR EFFECTS ON DYES REMOVAL AND BLOOD HEMOLYSIS .

A Thesis

Submitted to the Council of the College of Science, University of Kerbala,

in Partial Fulfillment of the Requirements for the Master Degree of

in Chemistry

By

Safaa Ali Khit

Supervised by

Prof. Dr. Eman Talib Kareem   **Assist.Prof. Dr.Ihsan Mahdi Shaheed**

2023 AD   **1445 AH**

بسم الله الرحمن الرحيم

﴿ وَيَسْأَلُونَكَ عَنِ الرُّوحِ قُلِ الرُّوحُ مِنْ أَمْرِ رَبِّي وَمَا أُوتِيتُمْ مِنَ الْعِلْمِ إِلَّا قَلِيلًا ﴾
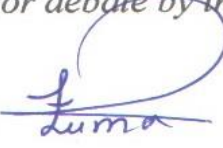
صدق الله العلي العظيم

سورة الأسراء
الآية ﴿ ٨٥ ﴾

Supervisor Certification

We certify that this thesis was prepared by **Safaa Ali Khit** my supervision at the Chemistry Department, College of Science, University Karbala, as a partial requirement for the degree of Master of Science in Chemistry.

Signature:

Name: **Dr. Eman Talib Kareem**

 Title: Professor

Date: 1 / 3 / 2023

Signature:

Name: **Dr. Ihsan Mahdi Shaheed**

Title: Asst. Professor

Date: 1 / 3 / 2023

In view of the available recommendations by the supervisor, I forward this thesis for debate by the examining committee.

Signature:

Name: **Dr. Luma M. Ahmed**

Title: Professor

Head of Chemistry, college of Science

Date: 2/3 / 2023

Examination Committee Certification

We certify that we have read this thesis entitled " **A green synthesis of copper oxide nanoparticles and study their effects on dyes removal and blood hemolysis** " as the examining committee, examined the student " Safaa Ali Khit" on its contents, and that in our opinion, it is adequate for the partial fulfillment of the requirements for the Degree of Master in Science of chemistry.

Signature:
Name:**Dr. Luma M. Ahmed**

Title: Professor
Address: University of Kerbala, College of Science, Department of Chemistry.
Date:2/3/2023
(Chairman)

Signature
Name: **Dr. Ennas Abdul Hussein**
Title: Assistant Professor
Address: University of Baghdad , College of Science for Women, Department of Chemistry .
Date:24 2/2023
(Member)

Signature:
Name: **Shaymaa Ibrahim Saeed**
Title: Assistant Professor
Address: University of Kerbala, College of Science, Department of Chemistry
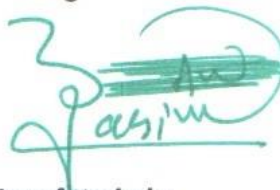Date: 26/ 2 /2023
(Member)

Signature:
Name: **Dr.Eman Talib Kareem**
Title: Professor
Address: University of Kerbala, College of Science, Department of Chemistry
Date: 1 / 3 /2023
(Member & Supervisor)

Signature:
Name: **Dr. Ihsan Mahdi Shaheed**
Title: Assistant Professor
Address: University of Kerbala, College of Science, Department of Chemistry
Date: 1 / 3 /2023
(Member & Supervisor)

Approved by the council of the College of Science

Signature :
Name: **Dr. Jasem Hanoon Hashim Al-Awadi**
Title: Assistant Professor
.Address: **Dean of College of Science, University of Kerbala**
Date:5/3 /2023

Dedication

To my father and mother

My precious wife

My beloved Children....

My Distinguished Professors

My brothers and sisters....

To all members of my family

To all friends and lovers

To every science students

I dedicate this study

Safaa

Acknowledgments

Praise be to **Allah**, Lord of the worlds, May God's blessings are upon **Mohammed** and his pure immediate family, and thanks to God for his countless and numberless graces and gifts.

I would like to extend my deep thanks, gratitude, and appreciation to:

My supervisor *Prof. Dr. Eman Talib Kareem and Assist.Prof.Dr. Ihsan Mahdi Shaheed* for their continuous support invaluable suggestions and great contributions since the very beginning of this work .

Also, I thank all faculty members of the Department of Chemistry in the College of Science at the University of Kerbala, for their worthless support of the research .

Finally, I thank my family and friends for their continued support throughout this journey. They were my source of encouragement along the way, I thank my best Friend and my brother *Ali Ameer*.

Safaa Ali Khit

Abstract

In this work, a green and cost-effective approach for producing copper oxide nanoparticles (CuO NPs) at room temperature utilizing *Anchusa strigosa L.* flower aqueous extract was described. UV–visible spectroscopy, Fourier transform infrared spectroscopy (FTIR), scanning electron microscopy (SEM), X-ray diffraction (XRD) and energy dispersive X-ray analysis (EDX-Elemental) methods were used to analyze the produced CuO NPs. Very stable, spherical particles were produced with an average crystal size of (28.22) nm. The CuO NPs were explored for their adsorption of Safranine and Gongo red dyes from aqueous solution . For the removal of two dyes utilizing CuO NPs, several batch experiment parameters, such as nanosorbent dosage, contact duration, pH, and ionic strength, were investigated . The isothermal equilibrum stoichiometric adsorption confirmed, the process data were examined by Langmuir, Freundlich , Temkin and Halsey adsorption equations at different temperatures (288-318K).The isothermal Freundlich and Halsey models gave a good linear relationship with the adsorption for Congo Red Safranin dyes using surface the CuONPs.The thermodynamic functions (ΔG, ΔH, ΔS) for the adsorption processes of safranin O and Congo red dyes on CuO NPs at different temperatures (288-318 k) were calculated. The change in enthalpy, ΔH, values obtained were(-23.1271) which means exothermal for Congo red, showing the adsorpation is the chemical adsorption, and (12.2731) which means endothermal for Safranin O, showing the adsorpation is the physical adsorption. Isotherms obtained from the experiments were identical to (4S-curve) in form at Giles' classification . The hemocompatibility of synthesized CuO nanoparticles was studied by hemolysis tests using human erythrocytes drawn from healthy volunteers.

Table of Contents

List of abbreviations and Symbols

(a,b)	Langmuir constants
AS	Absorbance of normal saline.
A_T	Temkin isotherm equilibrium binding constant
AT	Absorbance of test solution.
B	Temkin isotherm equilibrium constant related to heat adsorption (J.mol^{-1})
C_e	the equilibrium concentration of the adsorption solution in mg/l.
C_o	the initial concentration of the adsorption solution in mg/l.
CR	Congo Red dye
CuO NP	Copper oxide nanoparticles
CVD	Chemical vapor deposition
D	Crystallite size
EDX	Energy dispersive X-ray analysis
FTIR	Fourier transformation infrared
FWHM	The full-width at half-maximum
IUPAC	International Union of Pure and Applied Chemistry
JCPDS	Joint Committee onPowder Diffraction Standards
Keq	Equilibrium constant for the adsorption process at each temperature
K_F	Freundlich constant related with adsorption capacity (L / g)
K_H	Halsey isotherm constants
m	Mass of adsorbent (g)
n	Freundlich constant related with adsorption intensity
n_H	Halsey constants
PVD	Physical vapor deposition
Qe	The amount of adsorption at the equilibrium adsorbed concentration (adsorption capacity)(mg/g)
R	universal gas constant (8.314 J/mol K^{-1}).
R^2	Correlation coefficient
R_L	Separation factor
rpm	Cycle per minute
SA	Safranin-O dye
SEM	Scanning Electron Microscopy
T	Absolute temperature
UV-Vis	Ultra violet light in the range from 200 to 800 nm
V	Volume of the solution (L)
XRD	X-ray diffraction
ΔG	Gibbs energy (kJ/mol)
ΔH	Enthalpy (kJ mol^{-1})
ΔS	Entropy (J mol^{-1})
θ	The diffraction angle
λ max	The wavelength of maximum absorbance (nm)

CHAPTER ONE

Introduction

Chapter One
Introduction

1.1- Nanoscience

Nano mentioned in a Greek subscript which means 'dwarf' or whatever very tiny and shows a 1000 millionth of a meter (10^{-9} m) [1] as shown in figure 1.1 . Nanoscience is the study of molecules and structures in nanometer scales between 1 and 100 nm . As scientists figure out how to use the unique properties of atomic and molecular structures built at the nanometre scale, nanotechnology has become one of the most important areas of research at the beginning of the 21st century [2] .
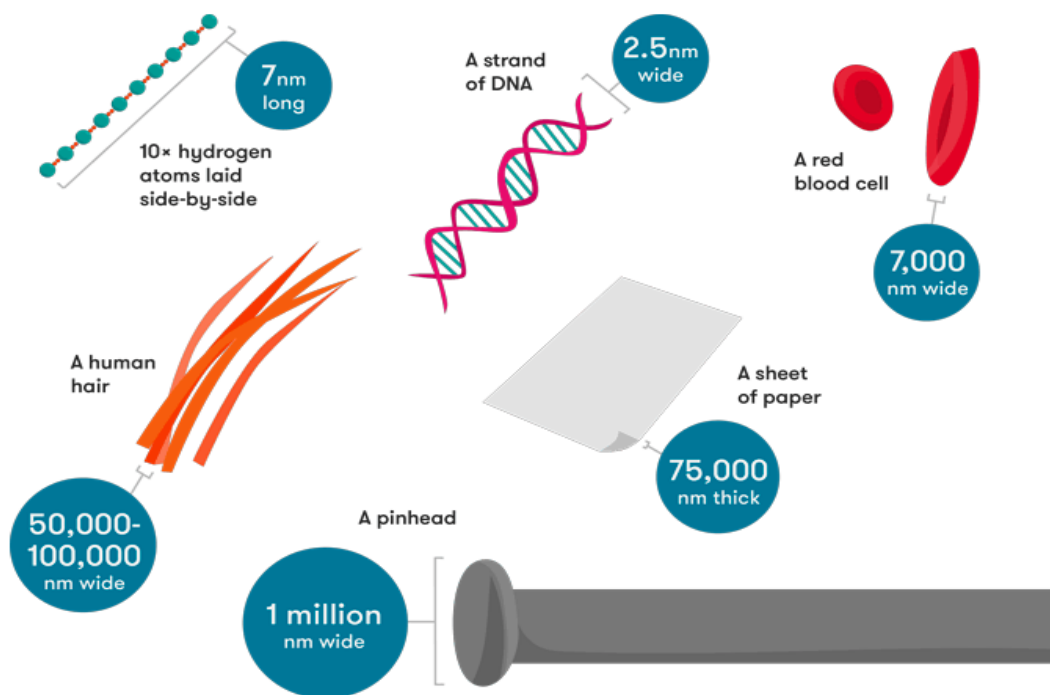
Figure 1.1 A correlation of magnitude of the nanomaterial[3]

1.2 Nanotechnology

Nanotechnology is what most people call the process of building and using functional structures that have at least one dimension that is measured in nanometres. At the Nano scale, the properties of matter are not always the same as those seen at larger scales. Important changes in behaviour are caused not only by the constant change of properties with decreasing size, but also by the

appearance of completely new phenomena like quantum size confinement, wave-like diffusion, and the dominance of interfacial phenomena. Once it is possible to change the size and shape of features, it is also possible to improve the properties of materials and the functions of devices beyond what is already known. Nanotechnology is an emerging application in various fields such as medicine, biofuel production, wastewater engineering, drug delivery, etc. (Figure 1.2)[4] .
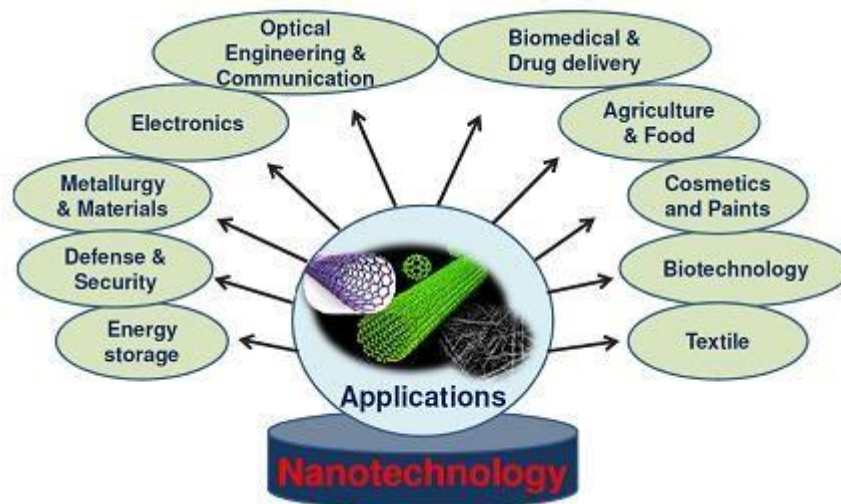
Figure 1.2 Application of nanotechnology in various fields

1.3 Nanomaterials

Nanomaterials which a single unit is sized (in at least one dimension) between 1 and 100 nm[5]. Materials with structure at the nanoscale often have unique optical, electronic, thermo-physical or mechanical properties [4] .

1.3.1 Classification of nanomaterial's

A variety of nanomaterials may be classified depending on a variety of criteria. The dimensions, condition, and chemical composition of Nanaomaterials are usually categorized according to their [6]. In addition, their classification is determined by their size, which ranges between 1 to 100 nm in at least one dimension, as illustrated in Figure (1-3) [7] .

Classification of Nanomaterials

(i) Dimensionality

0D

Solid nanoparticles

Hollow nanoparticles

Clusters

Quantum dots

1D

Nanorods

Nanowires

Fibres

CNTs

2D

Sheets layered nanostructured

Films

Patterned surfaces

Coatings

3D

Pillars

Electromechanical systems MEMS devices

3D composites

Polycrystals

(ii) Morphology

➤ Flatness,
➤ Sphericity,
➤ Aspect ratio

High-aspect ratio

Nanowires, Nanohelices, Nanozigzags, Nanopillers, Nanotubes, Nanofibers, Nanobelts

Low-aspect ratio

Nanospheres
Nanopyramides
Nanocubes

(iii) State

Isometric,
Inhomogeneous,
Dispersed, Suspension,
Agglomerate

(iv) Chemical composition

➤ Single constituent NPs
➤ Composites
➤ Inorganic & Organic
✓ Carbonaceous NMs
✓ Metallic NMs
✓ Branched dendrimers
✓ Quantum dots
✓ Ceramics NMs
✓ Semiconductor NMs
✓ Polymeric NMs
✓ Nanogels
✓ Core-Shell NMs

Figure 1.3 Diagrammatic representation of the categorization of nanomaterials according to several criteria.

1.4 Nanoparticles

Nanoparticles are particles with at least one dimension less than 100 nm; in the majority of instances, they are nanocolloids [8] . The various types of NPs include zero dimensional (0D)NPs, 1D nanowires, 2D nanosheets, and 3D networks[9]. The unique nanostructure of NPs, their physicochemical properties are substantially different from those of atoms and bulk crystals, as predicted by

Feynman in 1959 [10]. Their fascinating physicochemical properties account for the explosive growth of NP-based nanoscience and nanotechnology.The size effects that emerge as bulk crystals are transformed into NPs result in important changes in structural, spectroscopic, electronic, thermal, magnetic, mechanical, and chemical properties[11] .Because of their unique physicochemical properties,NPs have achieved great success in a wide variety of applications[12]. Considering catalysis as an example, the large surface-to-volume ratio and high density of low-coordinated atoms on the surface of NPs render them more active and attractive as catalysts. Reaction energy can be readily tuned to obtain the highest catalytic activity by controlling the composition, size, and shape of the NPs [12] .

1.4.1- Synthesis of nanoparticles

There are different methods for the synthesis of nanoparticles and these methods are divide into two main classes[13] as shown in Figure 1.4 .

1. Top-down method
2. Bottom-up method

1.4.1.1- Top-down method(Physical method)

This strategy employs a destructive approach. Starting with a bigger molecule, it is broken down into smaller components, which are then transformed into appropriate NPs. Based on the operation, response condition, and selected protocols, these methods are further split into several subclasses. This process includes grinding/milling, chemical vapor deposition, physical vapor deposition, and other decomposition methods[14] .

1.4.1.2- <u>Bottom-up method(Chemical method)</u>

Since NPs are created from comparatively simpler compounds, this strategy is also known as the "building up approach," since it is used in reverse. Examples include sedimentation and reduction procedures. This consists of sol gel, green synthesis, spinning, and biological synthesis [14] .
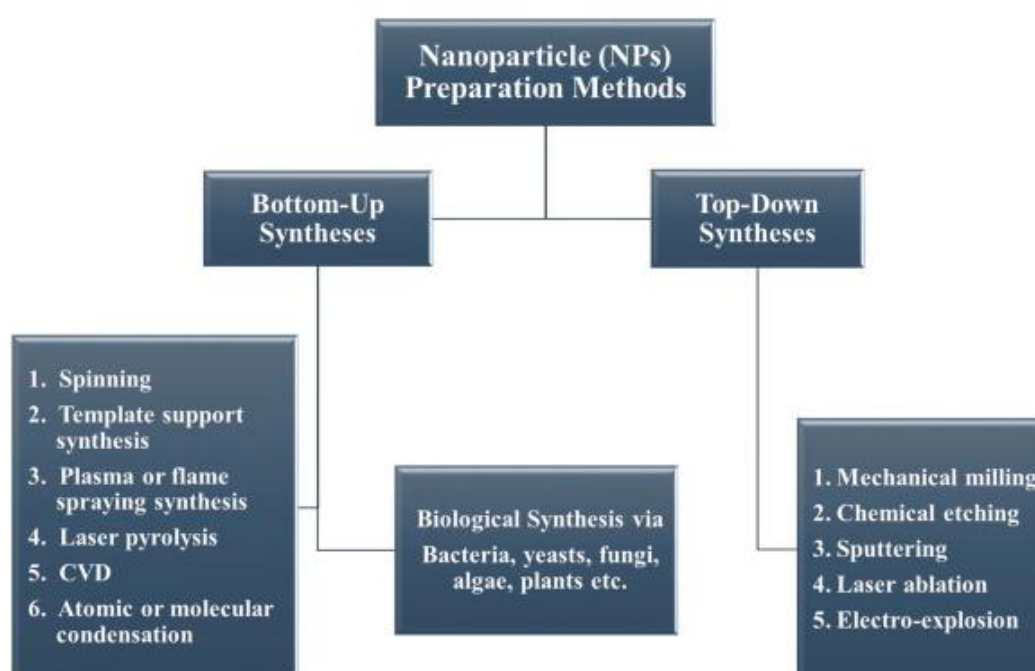
Figure 1.4 Typically synthetic methods for NPs for the (a) top-down and (b) bottom-up approaches [14] .

1.5- <u>Copper oxide nanoparticles</u>

Copper oxide is a compound composed of the periodic table block D and block P elements, copper and oxygen, respectively. In a crystal, four oxygen ions coordinate the copper ion. Copper (Cu) and copper oxide (CuO) nanoparticles have gotten a lot of attention because copper is an important and easy-to-find element in modern technology [15]. Copper nanoparticles are gaining popularity

owing to their optical, catalytic, mechanical, and electrical capabilities[16] . Copper oxide is used extensively in the fields of catalysis, superconductors, and ceramics as an essential inorganic element. It can be used as a catalyst and catalyst support, as well as electrode active materials, for example, in the nitrous oxide-ammonia degradation and the oxidation of carbon monoxide, hydrocarbons, and phenol in supercritical water [17]. Copper oxide nanoparticles are a powder that is soluble in dilute acids (NH_4 Cl ($NH_4)_2CO_3$, potassium cyanide solutions), insoluble in water, and slowly soluble in alcohols and ammonia solutions. It may be converted to metallic copper when heated in the presence of hydrogen or carbon monoxide. CuO nanoparticles may also be utilized as a catalyst for the rate of combustion in rocket fuel. Copper oxide nanoparticles have more catalytic activity and selectivity than copper oxide powder. The particle size of nanometer-sized copper oxide ranges from 1 to 100 nanometers. In comparison to regular copper oxide, nano CuO has distinct physical and chemical properties, including surface effect, quantum size effect superiority, volume effect, and macroscopic quantum tunneling effect in magnetic, optical absorption, chemical activity, thermal resistance, catalysis, and melting point .

1.5.1- Synthesis of copper oxide nanoparticles

  Several studies have documented numerous techniques for manufacturing CuONPs, such as chemical, physical, and biological synthesis. Figure 1.5 is a flowchart depicting the various CuONP synthesis procedures .
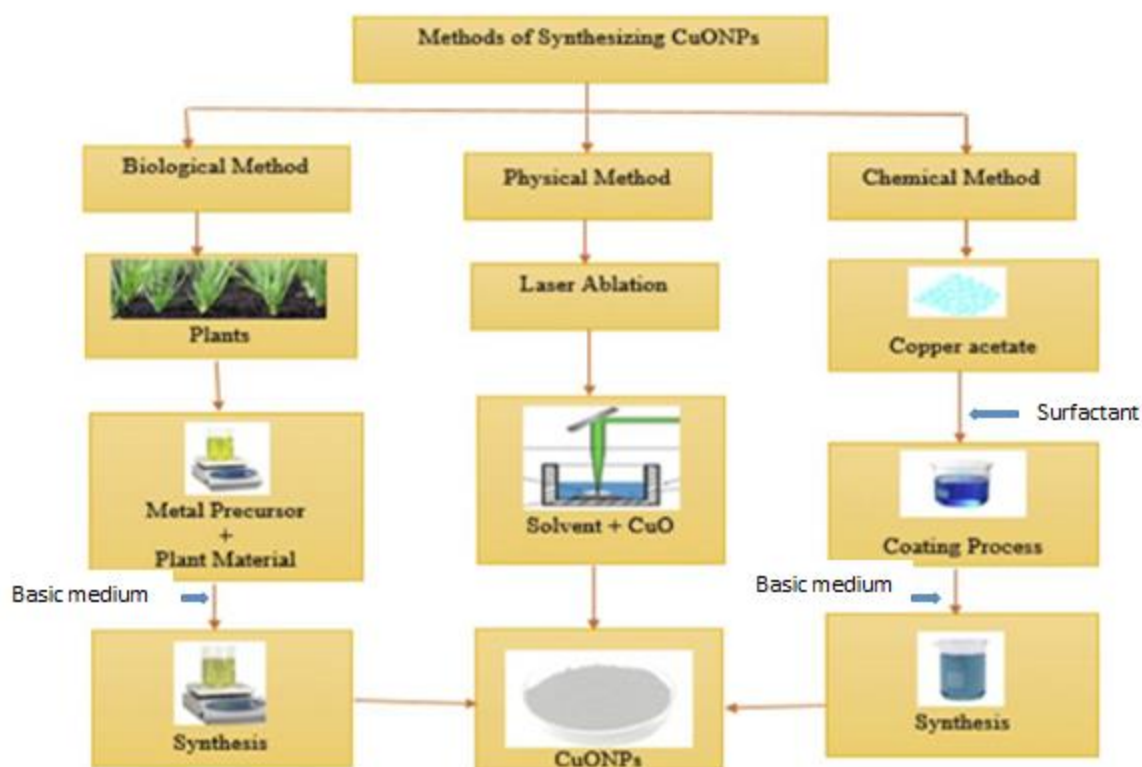
Figure 1.5. Flow chat representing the various methods of synthesis of CuONPs

1.5.1.1- <u>Chemical method</u>

This method requires the application of certain chemicals/reagents about the reduction of copper ions [18]. There are two types of chemical approaches to nanoparticle formation: the green chemical method and the conventional chemical approach. Organic substances, such as ascorbic acid, are manufactured the green chemical technique, In the usual method, inorganic chemicals such as sodium borohydride and potassium borohydride are used. Ascorbic acid can be used as a reducing agent in the making of CuONPs , and potassium borohydride can be used to make CuONPs [19]. Several studies [20] have shown that the chemical way of making CuONPs and other transitional metal oxide nanoparticles is very limited because it uses a lot of energy, pollutes the environment, uses high pressure and temperature, and uses expensive and dangerous chemicals .

1.5.1.2- Physical method

This approach utilizes an electric current as the electron source for the creation of necessary electrons during the synthesis of CuONPs [21]. Electrospraying, laser pyrolysis, laser ablation, and evaporation-condensation are the most frequently used procedures in the physical approach to CuONPs manufacturing. The pulsed laser-induced ablation approach has garnered the greatest attention among physical techniques since it is easy, ecologically friendly, and creates nanoparticles [22]. In the synthesis of CuONPs through laser ablation, a high-power pulsed laser is required and necessary for surface ablation. The manipulation of certain parameters, including pulse width, wavelength, laser source repetition rate, ablation time, and temperature, enables the synthesis of nanoparticles with the desired shape [23]. The benefits of the physical process include the manufacture of CuONPs with uniform, regulated dimensions and excellent purity [24]. Even though it has clear benefits, the physical method for making CuONPs is hard to use because it is expensive, hard to understand, and needs a lot of power and energy .

1.5.1.3- Biological method

The biological method for the manufacture of nanoparticles involves the use of organisms (bacteria, yeast, and fungus) and plant extracts as reducing agents for metal ions[25]. Researchers have found that Phormidium cyanobacteria, Organelle morgana [26], Serratia sp [27], and Escherichia coli [26] can all make CuONPs. Despite the eco-friendly benefit of manufacturing nanoparticles from microorganisms, its drawbacks include the toxicity of certain bacteria, difficulty in separation, and incubation processes [28]. But plants are still the best place to get metal and metal oxide nanoparticles. This is because plants can react quickly with little energy, they have a lot of biomolecules, they are cheap, they are stable,

they don't have any dangerous chemicals, and they are easy to use[29] . Biomolecules in plant extracts help make CuONPs and other metal nanoparticles by acting as both reducing agents and stabilizing agents [30] .

1.6- *Anchusa strigosa L.*

Anchusa strigosa is commonly known as (Lisan Althour) in Iraq. It is a member of the Boraginaceae family, which is often found in temperate, Mediterranean, and tropical climates; in Iraq, it grows along roadsides in the center and south [31]. Boraginaceae plants have naphthoaquinones, flavonoids, terpenoids, and phenols. Nevertheless, these plants contain hepatotoxic pyrrolizidine alkaloids [32]. In the past, Boraginaceae plants were used to treat fever, asthma, kidney stones, slow wound healing, arthritis, joint sprains or dislocations, and broken bones [33]. Flowers of *Anchusa strigosa L.*, brewed as tea: tonic for invalids and children; and reduce heart rate. It is a diuretic and diaphoretic substitute for *Anchusa officinalis* [33]. In Turkey, several Anchusa species have historically been utilized as wound healing and diuretic agents, while others have been used as demulcents, expectorants, analgesics, and sedatives[34]. In Jordan and Palestine, the decoction of the root is used as a diuretic, for stomach discomfort, and in the treatment of gastric ulcers, while the juice of the leaves is administered topically for skin diseases. arthritis and injuries [33] Different species of Anchusa extract have different pharmacological effects. For example, the high phenolic and flavonoid content of the methanolic extract of *Anchusa officinalis L.* makes it a good free radical scavenger[35] . While this action is beneficial for Anchusa strigosa aqueous extract [36] The anti-hyperglycemic effect of *Anchusa strigosa L.* in diabetic rats was followed by a considerable drop in fasting blood glucose and a rise in serum insulin levels, which may have resulted from an increase in pancreatic insulin production from existing cells or the release of insulin from its bound state[37] . An extract of *Anchusa strigosa* shows neuroprotective properties against amyloid toxicity, as well as decreased amyloid release from cells and -secretase activity [38]. At high concentrations, the

volatile oil of *Anchusa strigosa L.* displays potent antibacterial action against both Gram-positive and Gram-negative bacteria. *Anchusa strigosa* antioxidant activity owing to its phenolic and flavonoid levels may be advantageous for ischemia patients. In contrast, water and methanol extracts of *Anchusa strigosa* have anti-arthritic effects [39] .

Figure 1.6 Flower of *Anchusa strigosa*

1.7 Dyes and Water Pollution

Dye is an organic compound that imparts colour to substances such as textile fiber, leather, hair, plastic materials or wax either is solution or dispersion [40]. Dyes have long been known to man and in the prehistoric times they were derived from natural plants, mainly for colouring fabric. At present almost all the dyes are manufactured artificially even the natural dyes. The artificial dyes are thoughtfully delineated to have distinctive characteristics such as; ability to impart specific colour to the substance, resistance to fade when exposed to light, chemicals and washing [41]and resistance towards acids and bases. The groups that modify the ability of chromophores to absorb light are called auxochromes (NO_2, NO, N=N). The part of molecules which provides the colour by adsorbing wavelength is called chromophores (OH,NH_2, NHR, NR_2, Cl and COOH). Dyes can be broadly classified in two ways either based upon chemical composition or application. Dyes have a wide range of application and are used as a colorin agent for many different substances. Dyes are widely used to impart colour to fabrics

and plastics[40]. They are also used in food industry, printing and leather industry [42]. Recently, dyes have gained popularity in another field that is in hair coloring.[43]

1.8-Classification of Dyes

There are several ways to classify dyes. For example, they may be classified by fiber type, such as dyes for nylon, dyes for cotton, dyes for polyester, and so on. Dyes may also be classified 6y their method of application to the substrate. Such a classification would include direct dyes, reactive dyes, vat dyes, disperse dyes, azoic dyes, and several more types. These classifications are more suited to a book aimed at the technology of the application of dyes to a substrate rather than one dealing primarily with the synthesis and chemistry of dyes[44]

1.8.1-Congo red dye

Congo red ,the anionic coloring agent, has a chemical formula of $C_{33}H_{22}N_6NaO_6S_2$ with molecular weight of 696.7 g mol^{-1} . The IUPAC nomenclature [1-napthalene sulfonic acid, 3,3'-(4,4'-biphenylenebis (azo)) bis (4-amino-) disodium salt] Congo red (C.I. 22120) indicator Reag as shown in Figure 1.7. The diazo dye Congo red is made from tetraazotized benzidine and two molecules of napthionic acid. Congo red comprises the functional groups NH_2 and SO_3. In the presence of inorganic acids, the color of Congo red shifts from red to blue[45] .
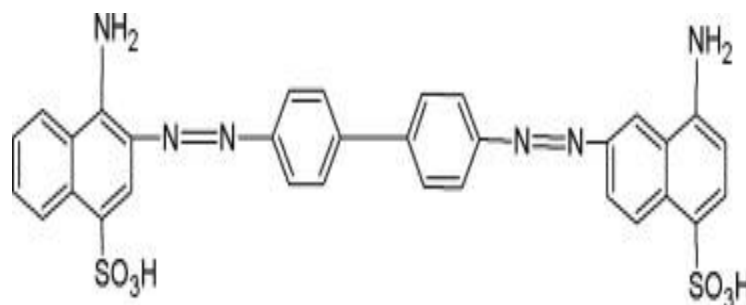
Figure 1.7 Structural formula for congo red dye [46]

1.8.2– Safranin-Odye

Safranin-O is a cationic red dye has a molecular formula $C_{20} H_{19} Cl N_4$ have molecular weight 350.85 g mol^{-1} with IUPAC name of 3,7-Diamino-2,8-dimethyl-5phenylphenaziniumchloride.Safranin-

O is one of the most frequently used synthetic dyes; it is a cationic azinedye . It is a wellknown textile dye used to

cotton, paper, wool, silk, and parbased fibers Safranin-O (C.I. 50240) indicator Reag [47].It is a water-soluble biopigment used in histology and cytology. Safranin is used as a contrast dye in some staining protocols, dyeing the cell nuclei a red color. It is considered a classic contrast dye used to stain endospores. It is used to detect cartilage, mucin protein produced by epithelial tissue cells, and mast cell granules [48]. The chemical structure of Safranin is shown in Figure 1.8 .
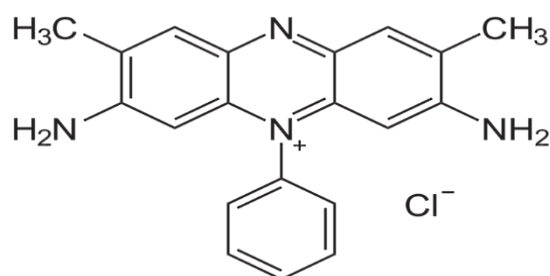
Figure 1.8 Structural formula for safranin-O dye [49]

1.9 - Adsorption

Adsorption is a process that occurs when a gas or liquid solute accumulates on the surface of a solid or liquid (adsorbent), forming a molecular or atomic film (the adsorbate)[50]. Adsorption is found in many natural, physical, biological and chemical systems and is widely used in industrial applications such as heterogeneous catalysts, activated charcoal, capture and use of waste heat to provide cold water for air conditioning and other process requirements (adsorption coolants), synthetic resins, increased storage capacity of derived carbon of carbide and water purification[51] .

1.9.1- Advantges of adsorption

Due to its high efficiency, rapid operation, and simple, adaptable design. Adsorption is one of the widely used ways for removing dyes from water . traditional approaches. In addition, the adsorbent is readily recoverable and reusable[41]. Due to its cheap capital expenditures and abundant availability of low-cost adsorbents, it is a cost-effective technology., adsorption is commonly employed for the removal of textile contaminants from wastewater. The adsorption process may not make any or very few harmful pollutants and is cheap to start up and run [52]. Environmentally, adsorption is harmless since no sludge is formed. Typically, the effluent generated after adsorption is of good quality [53]. In adsorption, the wastewater's contaminants adhere to the surface of the adsorbent. The physical and adsorptive properties of the adsorbate and the adsorbent describe how they interact with each other[54] . Physico-chemical processes are the most easy and practical of all color treatment methods. The treatment and disposal of sludge generated during the removal of dyes is a significant deficiency in the majority of physicochemical processes [53] . Due to its broad variety of applications, adsorption is the favored physicochemical technique. There are several inexpensive adsorbents available [52]. The ability of these low-cost adsorbents to pick up things can be easily increased by using simple and inexpensive methods .

1.9.2- Types of adsorption

Adsorption takes one of two forms, depending on the nature of the forces involved: physical adsorption (physisorption) or chemical adsorption (chemisorption) [55] .

1.9.2.1 <u>Physisorption</u>

Physical adsorption is a form of adsorption in which no electron transfer occurs between the adsorbent and the adsorbate. Due to the fact that physical adsorption needs no activation energy, the time necessary to reach equilibrium is quick. Also responsible for the non-ideal behavior of actual gases is physical adsorption [56]. It is distinguished by adsorption temperatures for the gas that are less than 40 kJ mol^{-1}. The adsorption process resembles the condensation of gas on liquid [57]. This indicates that the forces that hold the adsorbed gas molecules to the surface of the solid are comparable to the forces of cohesion between molecules in the liquid state. A rise in temperature increases the kinetic energy of molecules, causing them to depart the surface and diminishing the amount of adsorption. Physical adsorption is often seen when different gases stick to charcoal, no matter what the chemical makeup of the agent is [58] .

1.9.2.2 <u>Chemisorption</u>

The chemical adsorption (also known as Langmuir adsorption) happens only at the surface and includes genuine chemical bonding. Covalent adsorption is referred to as weak chemical adsorption, Strong chemical adsorption is referred to as ionic adsorption. Adsorbate and adsorbent will undergo a chemical reaction during this instance of adsorption. Chemisorption generates a single layer of adsorbate chemically bound to the adsorbent's surface. Similar forces that contribute to the formation of chemical compounds are responsible for chemical adsorption [59]. Chemisorption is irreversible due to the chemical bond between the adsorbate and the surface, which occurs during adsorption., it is often discovered that the original material has undergone a chemical transformation. Adsorption enthalpy is typically greater than 80 kJ mol^{-1}, indicating a high heat of adsorption . Physical and chemical adsorption characteristics for several parameters are compared in Table (1-1) .
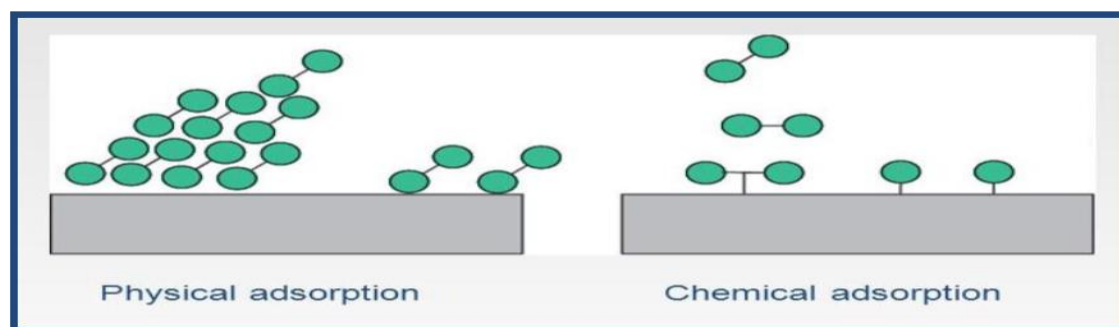
Figure 1.9 physical and chemical adsorption [60]

Table 1.1 Characteristics of physisorption and chemisorptions[61]

Physisorption	Chemisorption
Van der Waals, forces are the nature of forces.	The substance of forces is chemical bonding
The adsorption heat is less than 40 kJ mol^{-1}.	Adsorption heat exceeds 80kJ mol^{-1}
There is no electron transport or exchange between the adsorbed species and the surface of the adsorbent. Without the need for activation energy, the event takes place..	.Electrons are exchanged or shared between the surface of the adsorbent and the adsorbate. Energy for activation may be required
The procedure is generic.	The procedure is distinguished by its distinctiveness
Because the forces work over long distances, multilayer adsorption may occur.	. Adsorption results in the formation of a monolayer, which may be followed by inclusion
Adsorption is only detectable at temperatures below the adsorbate's boiling point.	Adsorption may take place at elevated temperatures
The process can be turned around. You can get rid of the adsorbing layer by emptying the area or heating it to a low temperature.	The process may be irreversible, resulting in a chemical reaction
The temperature of occurrence is typically low and is determined by the adsorbate's boiling point.	The temperature of occurrence is often high and is determined by activation energy.

1.9.3- Adsorption mechanisms in solution

Adsorption from solution onto a solid adsorbent is a complex phenomena; it varies from the adsorption of individual substances (gases, vapors, and pure liquids) in that the solution consists of at least two components that form a thick layer on the surface [62]. The adsorption of adsorbate molecules from the bulk liquid phase to the adsorbent surface is assumed to entail the following processes :

1. Adsorbate molecule transfer across the solid particle's boundary layer.
2. Adsorbate molecules spread from the particle surface to the active sites inside the pore-filled liquid as they traverse the solid surface of the pore.

3. Adsorption of solute molecules on the inner surfaces of pores' active sites..
4. After a molecule has been adsorbed, it may migrate on the pore surface through surface diffusion [63] .

1.9.4- Factors affecting adsorption process

The following factors affect the adsorption process:

1- Concentration of adsorbate

The quantity of material adsorbed by a given mass of adsorbent increases with increasing solute concentration at a constant temperature [64] .

2- Temperature

The effect of temperature on the adsorption extent depends on the type of adsorption and the nature of both adsorbent and adsorbate . according to the Lechatelier's principle, a decrease of temperature of the system would result in an increase of adsorption like, physical adsorption where a decrease in temperature enhanced the extent of adsorption like chemisorption [65] .

3- Ionic strength effect

The effect of ionic intensity on the adsorption process depends on the nature of the adsorbed material as well as the surface on which the adsorption process takes

place [66]. Sometimes the ionic strength leads to a decrease in the adsorption capacity and in other cases to an increase in the adsorption capacity. If the increase in the ionic strength of the additive reduces the solubility of the adsorbent, and this phenomenon is expected to occur when there are ions similar to one of the ions of the adsorbent material, which causes the effect of the combined ion that reduces the solubility of the adsorbent and thus increases the adsorption process [67] .

4- pH effect

Adjusting the pH of the solution has a considerable effect on the quantity of adsorption from the solution due to its influence on the chemical states of the adsorbent, adsorbate, and solvent. Due to the conflict between (H+) and (OH-) ions and their overlap with the adsorbent surface, adsorbate, or solvent, this effect is seen[68] .

5- Nature of the adsorbent

In this process, the percentage of adsorbent, chemical nature, pore size, and surface area all play a significant role in determining the level of adsorption [69]

6- Nature of adsorbate

The amount of adsorption depends on the chemical and physical characteristics of the adsorbate. How well a molecule can stick to a surface depends on its polarity, size, stereochemistry, and whether or not it has different persistent groups [70] .

7- Surface area of adsorbent

The surface area of a given mass of adsorbent is inversely proportional to the particle size. The more finely divided or porous a substance is, the greater its surface area and, thus, its absorption capacity. Thus, the increase in surface-active sites will lead to a rise in adsorptive capacity [71] .

8- Solvent effect and traube's rule

The solvent influenced the adsorption process's behavior, which may be represented in three interrelated ways:

1- The interaction between the solvent and the solute that contributes to solubility. In general, fewer soluble solutes would be more strongly adsorbed than more soluble solutes.

2- the chemical composition-dependent interaction between the solvent and adsorbent surfaces.

3- Interaction between the solvent and solute species in the adsorbed layer at the surface of the adsorbent [72] .

1.9.5- Adsorption isotherms classification

Adsorption isotherms refer to the relationship between the quantity of material adsorbed per unit mass of the adsorbent and the equilibrium (in the case of a gas) or concentration (in the case of a solution) at constant temperature. The study of the adsorption isotherm is crucial because it helps characterize the nature and circumstances of the adsorption process. It also helps figure out how much adsorbate is used and how concentrated it is during the adsorption process [73]. Giles and his coworkers observed and classified a number of phenomena. The illustration in Figure (1-10) illustrates adsorption on a solid active surface. Initial slope of the curve determines the major classification (S, L, H, and C). These classes include subclasses dependent on the solute concentration increase (1, 2, 3, 4, and maximum). Giles and his colleagues' classification revealed the following instances:

(I) S- curves ; If the solvent is strongly adsorbed, there is a strong intermolecular attraction inside the adsorbed layer, and the adsorbate is monofunctional, then a monofunctional adsorbate is formed [74] .
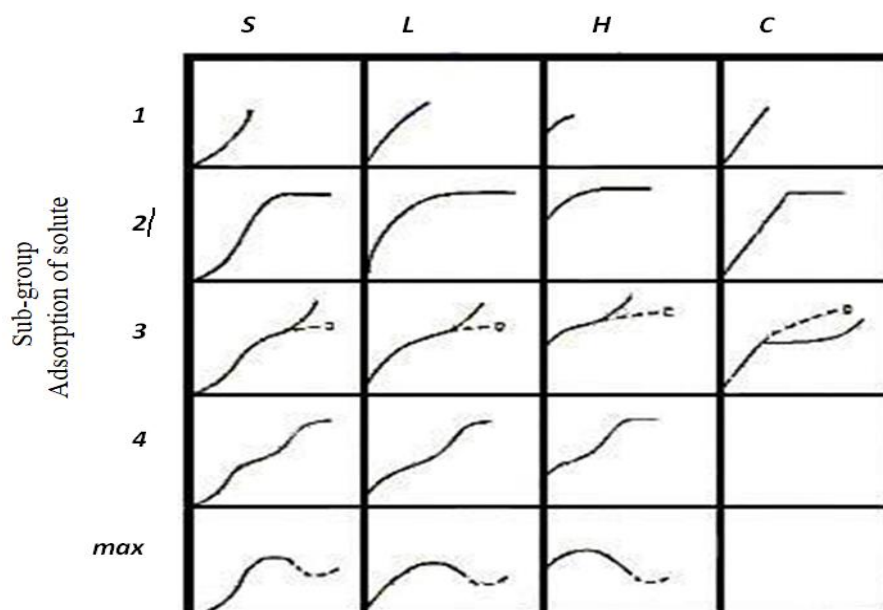
Equilibrium concentration of solution

Figure 1.10   Adsorption isotherm as in Giles classification

  (II) L- curves ; Langmuir-type compounds exist. It may be detected when there is minimal competition from the solvent for surface sites. Another theory is that the adsorbate molecules are long and flat, with their major axis parallel to the surface.

(III) H-curves ; When there is a substantial affinity between the adsorbate and the adsorbent, which is shown even in very diluted solutions, adsorption will occur. Consequently, it may be the result of chemisorptions, the adsorption of polymers, or the production of ionic micelles, but there are also other documented unique circumstances .

(IV) C- curves ; Examine the constant partition linear curves created by chemicals that enter the adsorbent quicker than they enter the solvent [74] .

1.10-Adsorption isotherms models

  There are several isotherm models available for describing the equilibrium sorption distribution. As the most relevant isotherms in adsorption from solutions, the Langmuir, Freundlich, Temkin, and Halsey isotherms will be described in depth [74] .

1.10.1- Langmuir isotherm

The Langmuir isotherm applies when just one layer of molecules may be adsorbed on the surface of the adsorbent. Monolayer adsorption is characterised by the fact that at moderate concentrations, the maximum quantity is adsorbed. As the concentration of the adsorbate increases, the surface of the adsorbent is continuously covered by a monomolecular layer of the adsorbate. The equation below shows Langmuir's formula : [75] .

$$Q_{e = \frac{x}{m}} = \frac{abC_e}{1+b\,C_e} \quad ....(1.1)$$

Where: Qe : Is the amount of adsorption at the equilibrium adsorbed concentration (mg/g), (C_e) : is the equilibrium concentration of the adsorbate (mg of adsorbate per liter of solution), (b) is the Langmuir constant related to energy of adsorption or equilibrium constant (L/mg), and (a) is the maximum adsorption capacity upon complete saturation of an adsorbent surface [76]

$$\frac{C_e}{Q_e} = \frac{1}{ab} + \frac{C_e}{a} ....(1.2)$$

Hall et al. (1966) [77] developed the dimensionless equilibrium term RL, commonly known as the separation factor, to describe the Langmuir constant b. The relevance of the R_L term is determined by the suitability of the provided data to the Langmuir isotherm model, beyond which the value of R_L gives crucial information on the nature of the adsorption isotherm, separation factor (R_L), estimated using the Langmuir isotherm model [77] :

$$R_L = \frac{1}{1+C\circ\,b} ....(1-3)$$

C_e is the equilibrium concentration of the adsorbate (mg of adsorbate per liter of solution), Utilization of the separation factor R_L to determine the kind of adsorption [78], which may be used to identify the geometry of an isotherm using Table data (1-2)

Table 1.2 value of separation factor

Value of R_L	Details regarding the absorption
$R_L > 1$	Unwanted
$R_L = 1$	Linear
$0 < R_L < 1$	Favorable
$R_L = 0$	Irreversible

1.10.2- <u>Freundlich isotherm</u>

It is feasible to describe experimental data over a restricted concentration range using the empirical isotherm proposed by Freundlich [79]

$$\text{Log } Q_e = \text{Log } K_F + \frac{1}{n} \text{ Log } C_e \ \dots\dots(1\text{-}4)$$

(Q_e) and (C_e) have the same significance as in Langmuir's equation. K_F adsorption capacity and n : adsorpation intensity are constants having no physical significance[79]. Equation (1.4), Nevertheless, it fails to predict the usual behavior seen at low and high dosages. In minute concentrations, (Q_e) is often directly proportional to (C_e) while at high concentrations(Q_e) has a fixed limiting value that is independent on (C_e). Equation gives the linearized version of this connection. (1.4) below:

A plot of log (Q_e) versus log (C_e) this function generates a straight line with a slope equal to ln K_F and a slope of (1/n).

1.10.3- <u>Temkin isotherm</u>

 The Temkin isotherm has a component that accounts specifically for species-adsorbent interactions. This isotherm assumes: (i) the adsorption is characterized by a uniform distribution of binding energies, up to a specified maximum binding

energy; and (ii) the heat of adsorption of all molecules in the layer declines linearly with coverage due to adsorbent-adsorbate interactions [80].

The Temkin isotherm is given as

Q_e = B ln ($A_T.C_e$)…………. (1-5)

Where ;

B :is the Temkin isotherm constant, computed as follows:

By rearrangement, the linear form of the equation may be derived. (1-7):

Q_e = B ln A_T + B ln C_e ………………..   (1-6)

By plotting Q_e versus InC_e, the values of b and A_T may be determined from the slope and intercept of the line.

Where : A_T = the binding constant for equilibrium.

B = connected to the adsorption heat [81].

1.10.4- <u>Halsey isothermal</u>

  The Halsey isotherm is used to evaluate multilayer adsorption at a relatively large distance from the surface[82], the Halsey isothermal model is the very good.

The Halsey isotherm fits the experimental data well due to high correlation coefficient(R^2), which may be attributed to the heterogeneous distribution of activate   sites   and   multilayer   adsorption. The Halsey equation has the following linear form: [83]

ln $Q_{e=}\dfrac{1}{n_H}$ ln K_H - $\dfrac{1}{n_H}$ ln C_e …………………..(1-7)

Where: K_H and n_H are the Halsey isotherm constants. The graph will be between of lnQe vs. lnCe

1.11- Hemolyses

Hemolysis is the breakdown or rupture of the red blood cell (RBC) membrane, which leads to the release of hemoglobin. Typically, the presence of free hemoglobin in red cell suspension media, such as plasma or additive solutions, is indicative of hemolysis in blood products. Certain disorders, such as hemolytic anemia, and procedures, such as blood centrifugation, might hasten RBC decomposition. Even though there have been big steps forward in making RBCs more stable during processing, storage, and transfusion, the risk of hemolysis goes up when RBCs are outside the body [84]. The presence of NPs in the environment has a significant impact on human health; thus, the combination of nanotechnology and toxicology has given rise to the new term "nanotoxicology." The release of metal ions from NPs is a major contributor to their toxicity. Both the release of metal ions from metal nanoparticles (NPs) and the environment to which the NPs are exposed play a significant role in the toxicity of the NPs [85] . CuO NPs binding, their interaction with live cells, and the resultant change in surface chemistry contribute to the misinterpretation of toxicity. To unravel the toxicity of CuO NPs, it is necessary to comprehend their characterization and surface modification, their routes of exposure, and the mechanisms or pathways involved in toxicity. Understanding the toxicity is complicated by the binding of NPs, their interaction with live cells, and the consequent alteration of the surface chemistry. To figure out how toxic nanoparticles are, you need to know how to describe and change the surface of NPs, how to get exposed to them, and what mechanisms and pathways are involved in toxicity [86]. Due to their minute size and tendency to release ions in acidic environments, copper oxide nanoparticles may be hazardous. To grasp toxicological pathways, the physicochemical features of any nanoparticle system are crucial. These characteristics include particle size, shape,

crystallinity, aggregation, and surface coating [87]. Copper is maintained in a state of homeostasis in the human body. If the quantity of copper ingested surpasses the human tolerance level, hemolysis, jaundice, and even death may result [88]. Red blood cells (RBCs) membrane mechanical stability is an excellent biomarker for assessing in vitro cytotoxicity as cells with cytotoxic chemicals. Lyses may result in a number of adverse health effects and illnesses. As a consequence of microbe activity, hemolysis has been documented in infectious disorders that are transmissible. Phenolic chemicals, flavonols, and glycosides have a variety of biological properties that may have a role in antioxidant and cytotoxic action [89]. Copper ions have been proven to have detrimental consequences, such as the generation of reactive oxygen species (ROS) that induce DNA oxidation and DNA strand breaks [90]. At high doses, copper has been shown to cause peroxidation of cell membrane lipids, lower the activity of cytochrome C oxidase, and interfere with mitochondrial respiration [91]. Theoretically, CuO NPs are much more hazardous than bulk Cu and other metal oxide nanoparticles [92]. Despite the widespread presence and use of CuO NPs in many organs and systems, little research has been undertaken to evaluate their immunotoxic effects; CuO NPs toxicity on human lymphocytes needs more study. This study evaluates the effects of CuO NPs on human lymphocytes and analyzes the processes behind the toxicity of CuO NPs towards human cells. NP penetration directly into cells, followed by intralysosomal dissolution and distribution of poisonous Cu^{+2} ions into the cytoplasm, seems to be responsible for the toxicity of CuO NPs in vitro rather than copper release in the growth medium[93]. In addition to accumulation, research has shown that NPs induce lysosomal destabilization and permeabilization of lysosomal membranes[94]. A limited permeabilization of the lysosomal membrane results in the production of reactive oxygen species, which induces cell death, while an extensive permeabilization induces cytosolic acidification and necrosis. Interference of NP with lysosomes may lead to

oxidative cell injury caused by reactive oxygen species (ROS), mitochondrial impairment, and decreased clearance of macromolecules (lysosomal malfunction) and damaged organelles (reduced autophagy) from cells. In this investigation, we examined the influence of CuO NPs on the lysosomal membrane integrity of human lymphocytes and observed the collapse of lysosomal membrane integrity after incubation with CuO NPs. The toxicity of CuO NPs to human lymphocytes raises concerns about their widespread usage and applications in the commercial sector. Given the health concerns, more study is necessary. This study is unusual since no earlier studies have studied the toxicity of CuO NPs on human normal cells, particularly human normal cells belonging to the human immune system, such as isolated human blood lymphocytes[90] .

1.12- Literature survey

In recent years, the development of an effective "green" chemical approach for manufacturing metal nanoparticles has been a key research priority. Green synthesis of CuO NPs is superior to chemical and physical synthesis because it is clean, non-toxic, cost-effective, and ecologically friendly. Plants high in bioactive chemicals used in the green synthesis of CuO NPs may act as a reducing, stabilizing, and capping agent during the NP synthesis process. Mixing a known concentration of plant extract with a known concentration of a precursor and heating the mixture to a defined temperature while continuously stirring is a popular method for generating CuO NPs (Table 1.3) .

Table 1.3 Green synthesis of CuONPs using plant extracts

S/N	Plants name	Salt	Applications	Size nm	Ref.
1	Tea	Copper nitrate	antibacterial activity	50-100	[95]
2	Tabernaemontana	Copper sulphate	Antibacterial	48 ± 4	[96]
3	Fortunella japonica	Copper sulphate	Sensing and remediation	5-10	[97]
4	Cissus quadrangularis	Copper acetate	Antifungal	30 ± 2	[98]
5	Rheum palmatum L.	Copper chloride	catalytic activity	10–20	[99]
6	Aloe Vera	Copper sulphate	Solar	24-60	[100]
7	Froriepia subpinnata	Copper sulphate	Remediation	6.95	[101]
8	Zea mays	Copper acetate	Antibacterial	36-73	[102]
9	Eupatorium odoratum	Copper sulphate	Antibacterial	10-20	[103]
10	Aloe barbadensis Miller	Copper sulphate	Degradation antibacterial activity	15-30	[104]
11	Eucalyptus globulus	Copper sulphate	Antibacterial	26-67	[105]
12	Camellia sinensis	Cupric acetate	Anticancer	22.44	[106]
13	Acalypha indica	Copper sulphate	cytotoxicity activity	26-30	[107]
14	Coleus aromaticus	Copper sulphate	Anticancer		[107]
15	Sida acuta	Copper sulphate	Antibacterial	26	[107]
16	Azadirachta indica	Copper acetate	anticancer activity	38	[107]
17	Hibiscus rosa-sinensis	Copper acetate	anticancer activity	15-25	[107]
18	Murraya koenigii	Copper acetate	anticancer activity		[107]
19	Moringa oleifera	Copper acetate	Antioxidant	6-61	[107]
20	Tamarindus indica	Copper acetate	Antioxidant		[107]

1.13- The aim of the study

This project's objectives are :

1- Green synthesis of CuONPs using some flower *Anchusa strigosa L.* Flowers extract .

2- Characterization of synthesized copper oxide nanoparticles CuO NPs .

3- Application of the prepreation CuO NPs as an adsorptive nanomaterial for purifying contaminated water from certain colors, as well as modeling the experimental findings using isotherm thermodynamic equations.

4- Study the Impact of synthesized CuO NPs on blood hemolysis.

CHAPTER TWO

Experimental

Chapter Two

Experimental

2.1. <u>Chemical materials</u>

Chemicals that were used in this study are listed in Table (2-1) .

Table 2.1: Chemicals used in this study

NO.	Chemical material	Purity	Company supplied
1.	Copper (II) Nitrate	99.9%.	Sigma-Aldrich Egypt
2.	HCl	35-38%,	Research since U.S.A
3.	NaOH	98.0%	Sdfcl U.S.A
4.	Ethanol	99%	Honeywell U.S.A
5.	NaCl	+98%,	Gerbu biotechnik Germany
6.	KCl	> 99.8%	Cephamlife sciences U.S.A
7.	$CaCl_2$	99%.	Spectrum U.S.A
8.	$MgCl_2$	99%.	Spectrum U.S.A
9.	Safranin-O Dye	98%	Himedia India
10.	Congo Red Dye	98%	Sigma-Adrich Egypt
11.	Triton-X 100	98%	Himedia India
12.	Normal saline	99%.	Pioneer-Iraq

2.2. <u>Instruments analysis</u>

Table (2-2) lists the instruments used in this investigation, along with their manufacturers and locations .

Table 2.2: Instruments used in this study

NO.	Instruments	Companies	Places
1-	UV – Visible Spectrophotometer Double Beam-1800	Shimadzu ,Japan	University of Kerbala, Science college
2-	Electronic Balance TP-214	Germany Denver	University of Kerbala, Science college
3-	FT-IR Spectrometers	Shimadzu,8400S Japan	University of Kerbala, Science college
4-	Thermo stated shaker GFL(D-300)	Germany	University of Kerbala College of Education for pure science,
5-	pH-450	Korea PHOENIK	University of Kerbala College of Education for pure science,
6-	Oven Memmert LOD – 080 + N	Labtech, Korea	University of Kerbala, Science college

7-	Scanning ElectronMicroscopy (SEM)	(kyky EM) 320., USA.	Isfahan University, Iranian Islamic Republic
8-	Hotplate Magnetic Stirrer	Heido-MrHei-Standard, Germany	University of Kerbala, Science college
9-	Blender	China	University of Kerbala, Science college
10-	(EDAX)Energy-Dispersive X-Ray (EDX) – Elemental Analysis in a Snap	Shimadzu, Japan	Isfahan University, Iranian Islamic Republic
11-	X-Ray Diffraction Lab X-XRD 6000, Spectroscopy	Shimadzu, Japan	Isfahan University, Iranian Islamic Republic
12 -	Microplate reader	BioTek (USA)	University of Babylon , Science college

2.3. Synthesis of copper oxide nanoparticles

2.3.1- Preparation of flower extract (*Anchusa strigosa)L.*

The flower petal of *Anchusa strigosa* was washed in distilled water and left to dry for two days in the lab room, the flower petal were ground, weighed (25 g) and melted in 100 mL of distilled water in the beaker and heated for 3 hours at 70℃, then filtered by Whitman filter paper(12) to collect the brown liquid of extract *Anchusa strigosa L.* flowers, Which were later used in the preparation of CuO NPs . Here lies the role of the extract prepared from the leaves of plants as a reducing agent by containing: A large amount of polyphenols, which in turn consist of flavonoids Flavonoids, antibiotics, antioxidants, organic compounds, and when this is added The extract from copper salt breaks the (OH) bond and is partially bonded with the metal. When this is broken The partial bond transfers electrons to form copper hydroxide, which in turn reacts with (OH), coming from sodium hydroxide, to be nanocrystalline copper oxide.

2.3.2- Green synthesis of copper oxide nanoparticles

(35 g)   Copper(II) nitrate was dissolved in 100 mL of distied water at 25 ℃ for 5 min. The extract was added to a solution of copper (II) nitrate dissolved in water, leached and dried in the incubator at 100 ℃ for a 1 hour. As shown in Scheme   2.1 .

washing and drying

grinding

addition (5 g) powder + 100 mL D.W heated at 70 oC for 30 min.

addition 80 mL of extract

NaOH

addition 5 g of $Cu(NO_3)_2$ + 100 ml of D.W. at 70 oC for 3 hours

filtering

extract

filtering and washing by Ethanol + D.W.

at 100 oC at 1 h

CuO-NPS
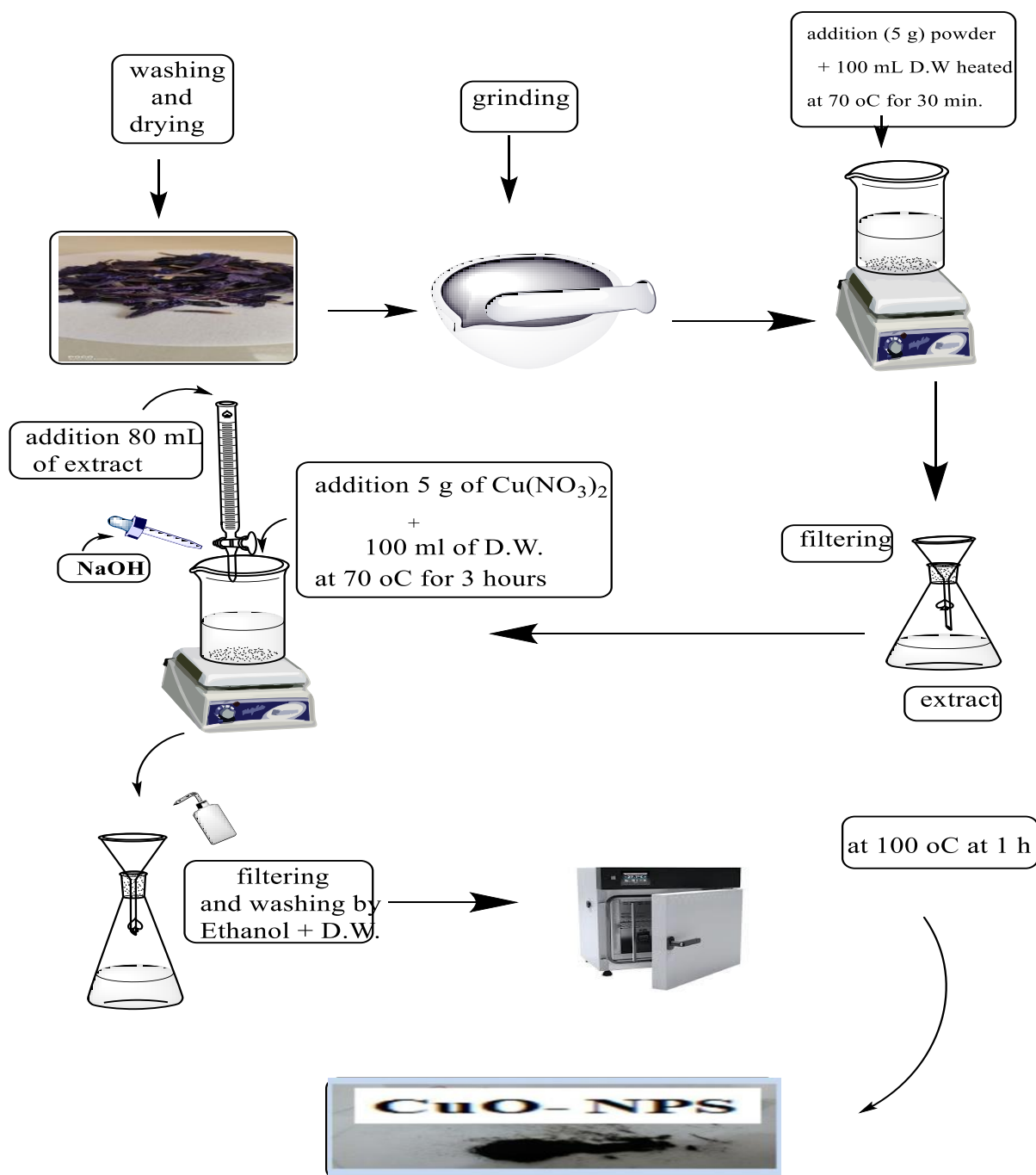
Scheme 2.1 Schematic Diagram for preparation of copper oxide nanoparticles

2.4- Determination of λ $_{max}$ and calibration curves for each dye

The maximum wavelength of (Congo Red and Safranin-O) dyes was specified by using spectrophotometer in the range of (200-800nm) ,and recording the spectra of absorption as shown in the Figures 2.1 and 2.2 . It is found that the highest absorbance of the Congo Red dye at wavelength λmax at (495 nm), and prepared solution of Safranin-O dye at wavelength λmax at (530 nm) .
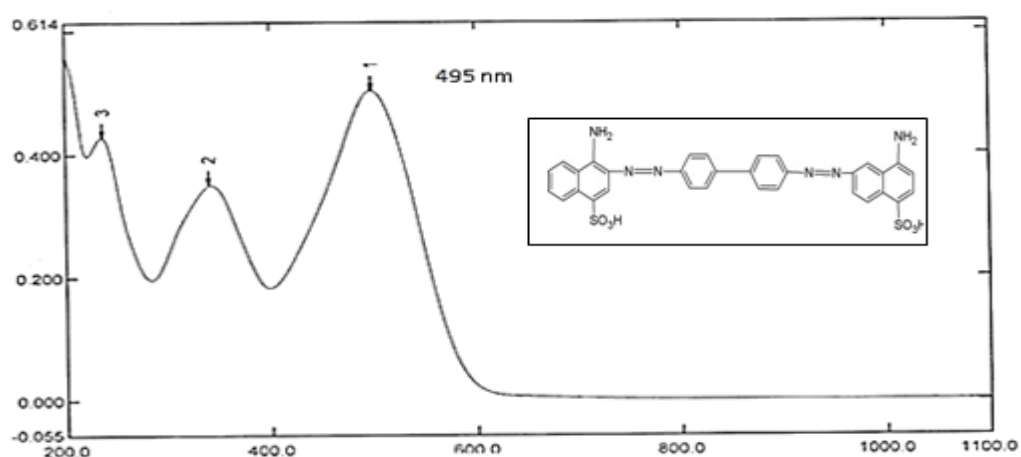
Figure 2.1 U.V.Visble Spectrum for congo red dye
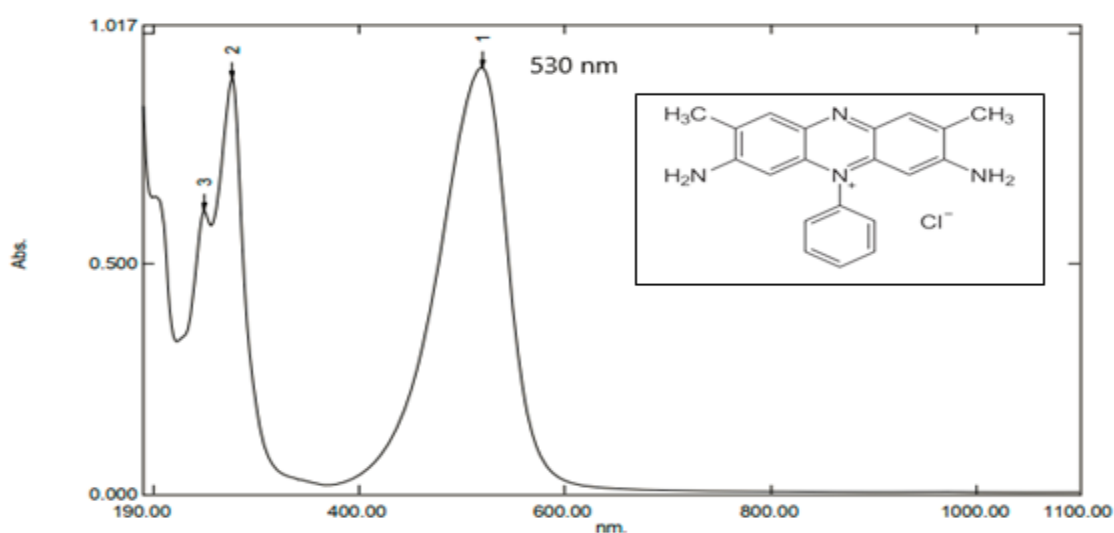
Figure 2.2 U.V.Visble **Spectrum for safranin-O dye**

Figures 2.3 and 2.4 show calibration curve of (CR) and (SA) dyes respectively .
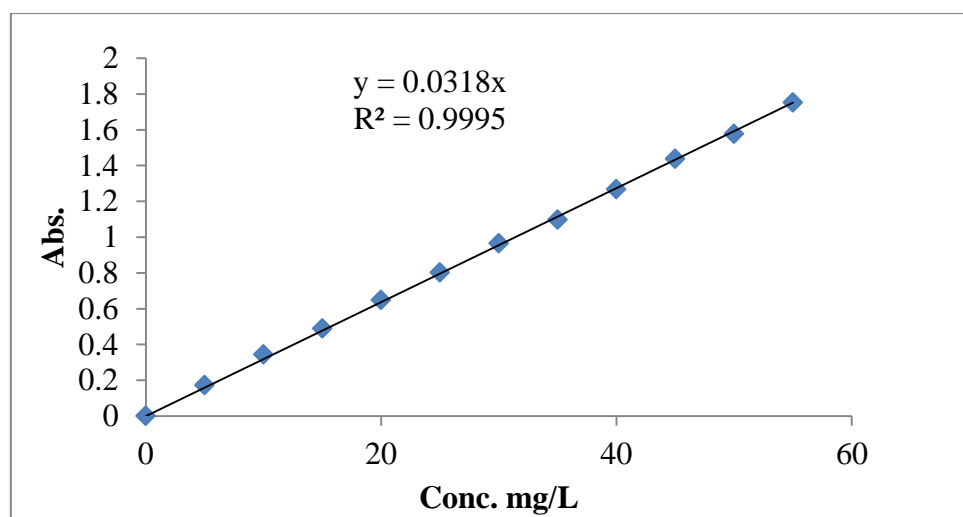
Figure 2.3 Calibration curve of congo red dye solution at 495 nm at pH = 3
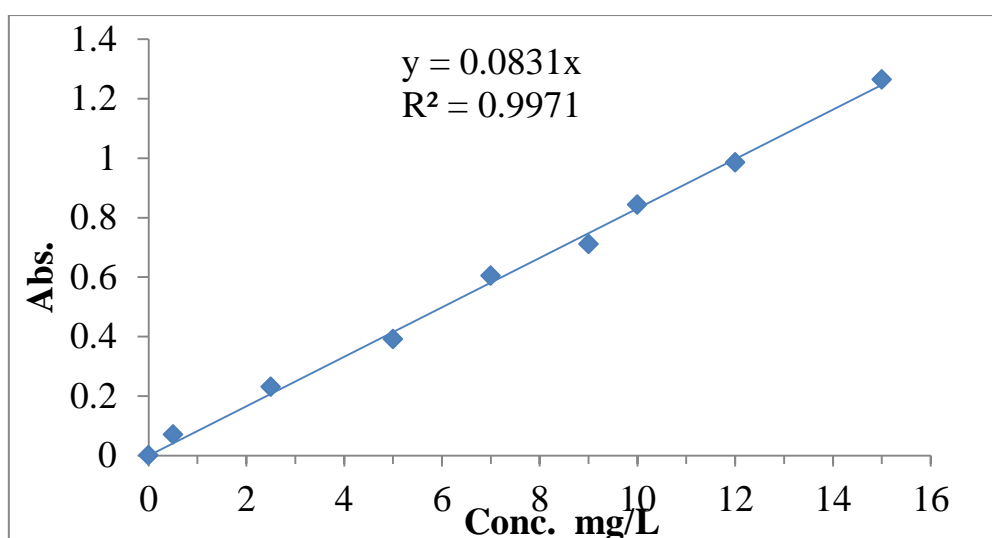
Figure 2.4 Calibration curve of safranin-O dye solution at 530 nm at pH = 9

2.5- Equilibrium time of adsorption system

For the study of the time required to achieve equilibrium between the adsorbent surface and the adsorbant, volumetric flasks with a capacity of 25mL used a concentration of 35 mg/L for Congo Red dye with 0.0300 g of (CuO NPs) and a concentration of 12 mg/L. Safranin-O dye with 0.0100 g of (CuO NPs). The Shaking prouss was carried out at different times ranging between (5-120) min,the solutions were filtered, and the absorbance was measured at the maximum wavelength of 495 nm and 530 nm for each of the two dyes respectively.

2.6- Adsorption isotherm

The adsorption isotherm for two dyes with the adsorbent surface (CuO NP), different concentrations were used, ranging from (5.0000-55.0000) mg/L) of Congo Red dye and different weights between (0.0050-0.0700) g for (CuO NPs) pH was then set to = 3 . For Safranin-O dye, concentrations ranging were used from (0.5000–15.0000 mg/L) with different weights between (0.0050–0.0700) g for (CuO NPs) , adjusting the acidity function within (pH =8) and using the flasks were shaken at a constant speed of 180 rpm in a thermostatically controlled shaker for the desired temperatures within the range (288–318 K). These solutions were filtered, and the absorption was measured at the maximum wavelength of each dye, using a UV-visible device. Then the concentration of each dye was found at equilibrium (Ce mg/L) based on calibration curves , as shown in the following equation:[108] .

$$Q_e = \frac{V(C_0 - C_e)}{m} \ \dots\dots\dots(2\text{-}1)$$

$Q_e =$ adsorption capacity in mg/g.

$C_e =$ the equilibrium concentration of the adsorption solution in mg/L.

$C_o =$ the initial concentration of the adsorption solution in mg/L.

$V =$ total volume of the adsorption solution in units L.

$m =$ weight of the adsorbent in g.

The removal percentage of the two dyes (R%) was also calculated using the following equation [109].

$$R\% = \frac{C0 - Ce}{C0} \times 100\% \ \dots\dots(2\text{-}2)$$

$R \% =$ The removal percentage

2.7- Analyze factors affecting the adsorption process

2.7.1- Effect of adsorbent weight

The change in the weight of adsorbent surface has an effect on adsorption, so it was studied using a concentration of 35.0000mg/L and 12.0000mg/L with

shaking time of (30 min and 20 min) for Congo Red and Safranin-O, dyes respectively, by different weights of the absorbent surfaces, ranging from (0.0050-0.0700g) for CuO NP at (298K). These solutions were separated with a centrifuge, then filtered, and the absorption at the maximum wavelength of each dye was measured with a UV-visible device. After that, the concentration of each dye at equilibrium (Ce mg/L) was found based on the calibration curves that had already been made, which was used to figure out the percentage of removal .

2.7.2- <u>Effect of pH</u>

The effect of changing the acidity function on the percentage removal and the adsorption process was studied by using concentrations of 35.0000 mg/L and 12.000 mg/L of Congo Red and Safranin-O dyes tested in various pH medium NaOH (0.1 N) and HCl (0.1 N) were used to adjust the pH within the range of (2–12), and then the identical steps as in (2.7.1) were carried out .

2.7.3- <u>Effect of ionic strength</u>

The effect of ionic strength on adsorption capacity and removal percentage was studied by using different concentrations ranging between (0.0200-0.0700 M) of salts (NaCl , KCl, $MgCl_2$ and $CaCl_2$), with concentrations of 35.0000 mg/L and 12.000 mg/L of Congo Red and Safranin-O dyes were used, respectively, while fixing the optimal conditions for the adsorption process. Then the same procedures mentioned in the previous paragraph were used in (2.7.1) .

2.7.4- <u>Effect of temperature</u>

To determine the fundamental thermodynamic functions, adsorption experiments were conducted at temperatures (288, 298, 308, and 318)(K) in the same way as described in Section 2.7.1 .

2.8- <u>**Hemolytic assay**</u>

This test used the blood hemolysis technique, which is an in vitro disruption of human red blood cells (RBCs) by CuO NPs, as well as blood samples from sixty healthy, nonsmoking volunteers between the ages of 18 and 45 [110].

1- A (15) μL of CuONPs or extract solution at various concentrations (0.1 and 0.3) μg/mL. The appropriate substances were added to 0.1 mL of blood sample and well mixed for 5 seconds.

2- To avoid excessive hemolysis, 10 mL of normal saline were added.

3- For ten minutes, the mixture was centrifuged at 3000 rpm.

4- At 540 nm, the mixture's absorbance was measured.

5- Completed the hemolysis (100%) was obtained by diluting blood with 100 times its original volume of distilled water.

6-Triton X-100 was used as a control.

After measuring absorbance, the percentage of hemolysis was calculated using the following formula:[111]

$$\textbf{\% Hemolysis} = \frac{(AT-AS)}{(A\ 100\%-AS)} \times \textbf{100 \%} \quad ....(\textbf{2-3})$$

AT: Absorbance of test solution.

AS: Absorbance of normal saline.

A 100%: Absorbance of 100% hemolysis.

2.9- <u>**Characterizations of the prepared nanomaterials**</u>

The synthesized samples in this study were characterized by using several techniques, Fourier transform infrared spectroscopy (FTIR) , X-ray diffraction (XRD), Field emission scanning electron microscope (FE-SEM), Energy Dispersive X-ray Analysis (EDX-Elemental) .

2.9.1-<u>**Fourier transform infrared spectroscopy (FTIR)**</u>

Fourier transform infrared spectroscopy (FT-IR) spectra were recorded on the Spactra FTIR-2, Perkin Elmer Instrument (using the potassium bromide

KBr pellets method at room temperature) to figure out what the functional

groups in CuO NPs and flower extract were [112] .

2.9.2- <u>X-rays diffraction patterns (XRD)</u>

X-ray diffractometer were employed to determine the particles size of prepared nanomaterial. The diffractograms of nano-materials provide information about crystallite size phase composition, crystallographic orientation and lattice strain, the lattice planes in a crystal are separated by a distance (d) . Braggs' law relates the wave length (λ) of the reflected X-ray, the spacing between the atomic planes (*d*) and the angle of diffraction *(θ)* as follows: [113]

$$n\lambda = 2d \sin\theta \ldots\ldots (2\text{-}4)$$

The calculation of the crystal structure and crystallite size of the synthesized materials at room temperature by the Debye - Scherer's formula in the follo-wing equation: [113]

$$D = \frac{K.\lambda}{\beta.Cos\theta} \quad \ldots\ldots\ldots (2\text{-}5)$$

Where: *D* is the average crystal size, *k* is the shape factor with a value close to unity 0.94 for homogeneous shape and 0.89 for heterogeneous shape $\lambda = 0.154$ nm is the X-ray wavelength of (*$Cu_{k\alpha}$*), *β* is the full width at half-maximum intensity (FWHM) of the diffraction peaks and *θ* is the Bragg's angle of the peak [114].

2.9.3- <u>Field emission scanning electron microscopy (FE-SEM)</u>

Field emission scanning electron microscopy (FE-SEM) technique used revealed the surface morphology properties of prepared nanomaterial; the specimens were analyzed by a field emission scanning electron microscope (FE-SEM, Zeiss, Germany) at electron high tension EHT 10 Kv and 60 kx magnification[112]

2.9.4-<u>Energy dispersive X-ray analysis (EDX-Elemental)</u> :

This technique is used to give information about the composition of an

element. As a result of passing an electron beam through the atoms of the

sample, spectraum of each element is obtained. This technique correlates with

the scanning electron microscope [115] .

CHAPTER THREE

Results & Discussion

Chapter Three

Results and Discussion

3.1- Characterization of CuO NPs

3.1.1- FT-IR analysis for flower extract (*Anchusa strigosa)L.*
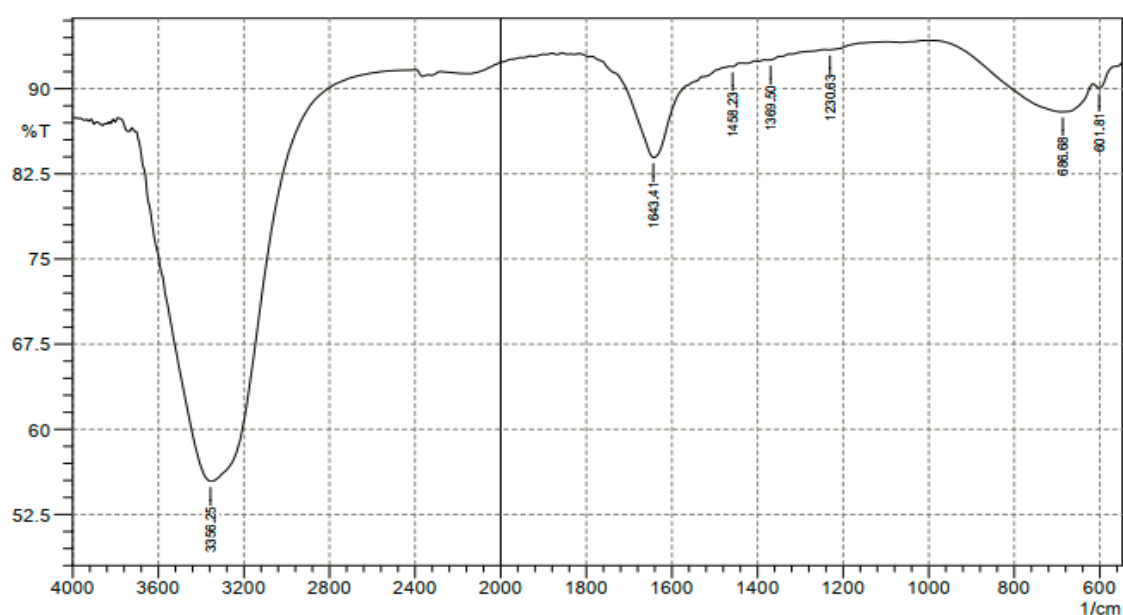
Figure 3.1 FT-IR spectrum of flower extract (*Anchusa strigosa*)

Figure 3.1 depicts the FTIR spectrum of flower extract (*Anchusa strigosa*) L. Which reveals a wide absorption peak at 3356 cm^{-1} owing to stretching vibrations of O–H bonds in a carboxylic acid [116] . The vibration of the C=O bonds produced absorption bands at 1643 cm^{-1} in the spectraum. Similar to the C=O bonds in carboxylic acids, two absorption bands at 1458 cm^{-1} and 1392 cm^{-1} may be attributed to the stretching vibration of C=O bond [117] . The absorption peak at 1230 cm^{-1} is caused by the stretching of carboxylic C–O bonds [118] .

3.1.2- FT-IR analysis for copper oxide nanoparticles

FT-IR spectrum of synthesized CuO NPs using the *Anchusa strigosa L.* flower aqueous extract is shown in Figure 3.2 .
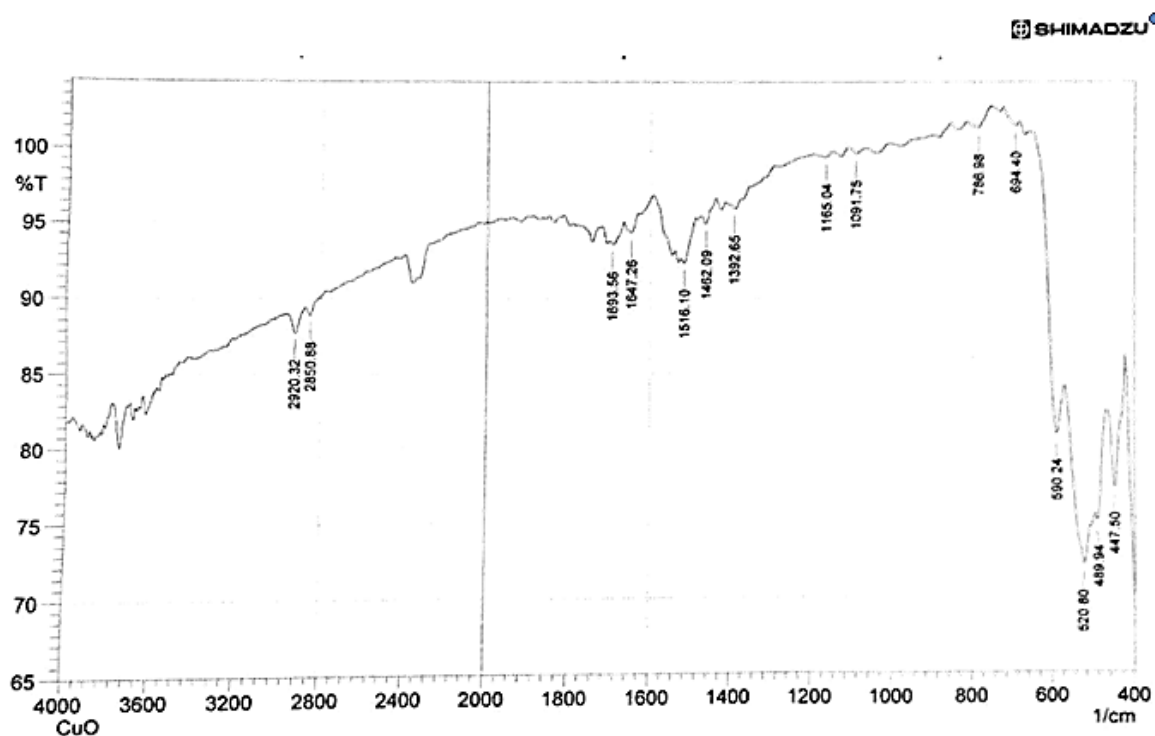
Figure 3.2 FT-IR spectrum of CuO NPs.

The peaks at 2920 and 2850 cm^{-1} were assigned to C-H stretching, and the peaks of the bands at 1647 cm^{-1} and 1693 cm^{-1} have been reported to be indicative of the C=C stretch of alkenes and the C=O stretch of the carbonyl in amides[119]. The peak at 1516 cm^{-1} 1452 cm^{-1} were C=C aromatic groups[120]. The peak observed at 1091 cm^{-1} was due to the strong C-O stretching [121] . The peaks at 489 and 447 cm^{-1} result from the CuO stretching modes [122] .

3.1.3- XRD analysis for CuO NPs

XRD analysis of the synthesized CuO NPs by extracted flowers of *Anchusa strigosa L.* aqueous extract was illustrated in Figure 3.3.
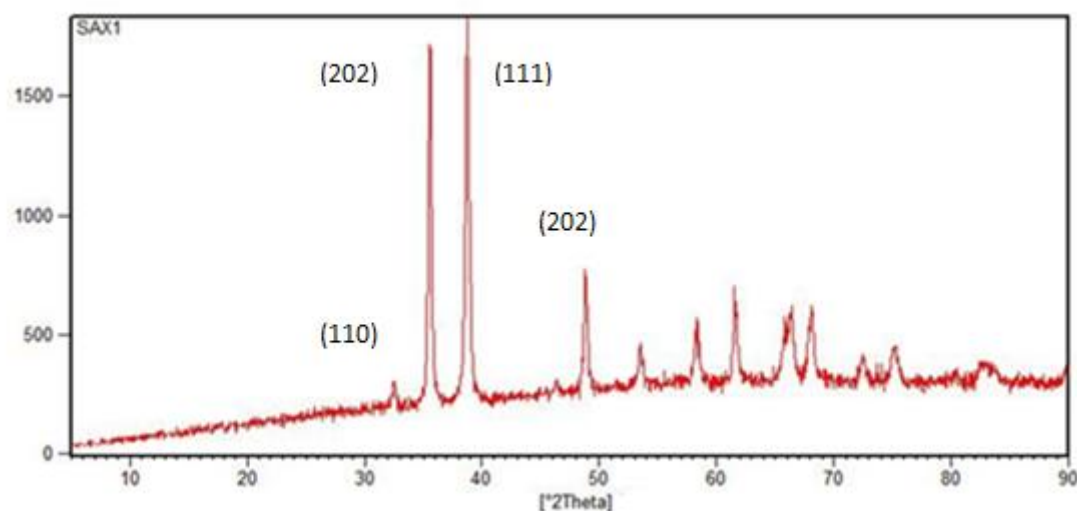
Figure 3.3 X-RD spectrum of CuO NPs.

The X-RD data were recorded in terms of the diffracted X-ray intensities (I) *vs.* 2θ . The crystalline size was calculated with the help of Scherer's formula, which is given as [113]

$$D = \frac{0.9\lambda}{\beta \cos\theta} \quad \ldots\ldots\ldots\ldots(3\text{-}1)$$

The crystal size of CuO particles can be obtained by using Scherer's formula = 28.22 nm .

XRD analysis of the synthesized CuO NPs by flowers of *Anchusa strigosa* L. aqueous extract was illustrated in Figure 3.3 . The 2θ peaks at $33.3°$, $36.2°$, $38.4°$, $49.1°$, $53.4°$, $58.4°$, $62.2°$, $65.8°$ and $67.2°$ are attributed to the crystal planes of copper oxide at (110), (002), (111), (202), (020), (202), (113), (311) and (113) respectively[122]. The copper oxide nanoparticles (CuO NPs) are well crystalline , the position and the relative intensity of the diffraction peaks match well with the standard phase CuO NPs diffraction pattern of the International Center of Diffraction Data card(JCPDS) .

3.1.4 <u>**FE-SEMS for CuO NPs**</u>

The SEM micrograph of the (synthesized CuO NPs using the extract of flowers *Anchusa strigosa L.)* is illustrated in Figure 3.4 . This indicates that the produced CuO NPs were mostly spherical and seemed more aggregated. This

may occur as a result of the coating of various surface functional groups by the extracted [123] .
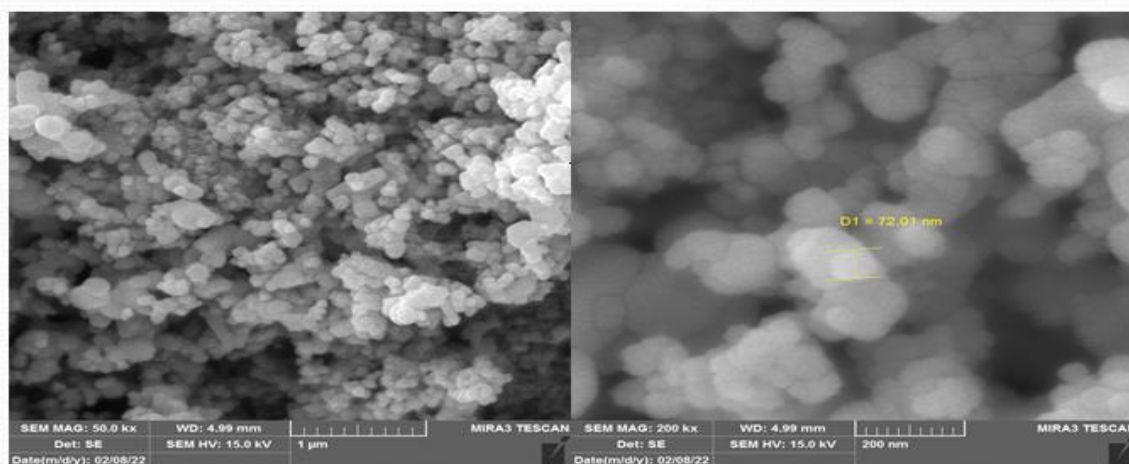
Figure 3.4 SEM photography of CuO NPs

.

3.1.5- EDX analysis for CuO NPs

EDAX determines the elemental component of CuONPs and other metal nanoparticles. X-rays are produced when an electron beam from EDAX impacts CuONPs [124]. Subjective and quantitative evaluations are performed on the emitted X-rays. Quantitative analysis determines the concentration of different elements in CuONPs based on the intensities of the peaks, while qualitative analysis determines the positions of each X-ray peak on the EDAX spectrum [125]. Modern technology improves the connection of EDAX to SEM for trace element detection and quantification. EDAX is able to measure atoms with atomic numbers ranging from (4 to 92) [126]. EDAX spectrum is shown in Figure 3.5 . Energy dispersive X-Ray analysis of CuONPs can be used to calculate the stoichiometric ratio and chemical component of CuO NPs. The percentage of copper and Oxygen obtained from EDAX is O 23.2 wt.. % and Cu 76.8 wt. %. Also, no characteristic peaks of impurities are observed .
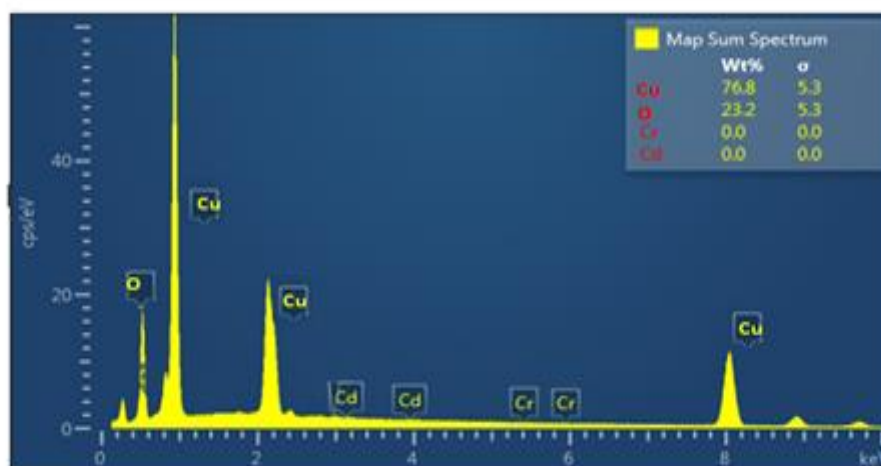
Figure 3.5 EDX spectrum of CuO NPs.

3.2- Study Factors influencing on Removal of CR and SA Dyes

This part includes the various investigations that could elucidate all the factors affecting the utilization of the CuO NPs in the removal of Congo red and Safranin-O dyes pollutants from water. Furthermore, the work includes the adsorption isotherms, the theoretical models that describe the isotherms, and the thermodynamics of the adsorption process .

3.2.1- Equilibrium time

The contact times between the adsorbents (CuO NPs) and fixed concentrations of CR and SA dyes (35.0000 mg/L and 12.0000 mg/L) as adsorbate that are sufficient for the adsorption process to reach equilibrium at 298 K were studied at different periods (10, 20, 30, 40, 50, 60, 80, 100, and 120 min). until reaching equilibrium. Equilibrium times of adsorption systems were studied here at 30 min and 20 min. These were the best equilibrium times for Congo Red and Safranin, respectively. The results are shown and summarized in Figure 3.6 and Table 3.1 .

Table 3.1 Effect of equilibrium time on adsorption CR and SA dyes on CuONPs at 298K.

Time/min.	Removal %= $\frac{C_0 - C_e}{C_0} \times 100$	
	Congo Red	**Safranin**
10	96.1365	94.7854
20	96.3162	95.1865
30	96.9451	95.0862
40	96.5858	94.1837
50	96.8553	94.1837
60	96.8553	93.6823
80	96.8553	93.5820
100	96.8553	93.5820
120	96.8553	93.5820
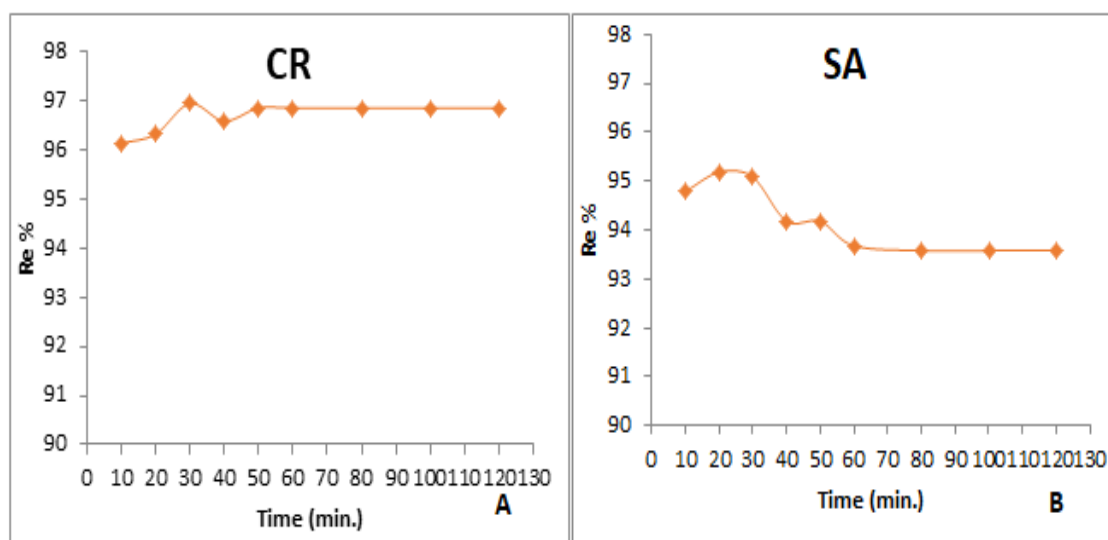
Figure 3.6 Effect of contact time on adsorption of CR and SA dyes on the surface of CuONPs at 298 K.

3.2.2- <u>Effect of surface weight</u>

Effect of adsorbent dose change adsorption process of CR and SA dyes on(adsorbent) CuO NPs was studied by using a fixed concentration of (35.0000 mg/L) of CR dye and (12.0000 mg/L) of SA dye and different weights of adsorbents ranged between (0.0050-0.0700 g) at 298K. Figure 3.7 and Table 3.2 demonstrate the influence of the adsorbent weight change on the adsorption quantity for CR and SA dyes.The removal rate of the two dyes increases with the increase in surface weight, and the reason is the additional area that contains an increase in the number of (active sites)[127] . Until it reaches a specific value that represents the amount of the adsorbate in the saturation stage and is not affected by the increase in the weight of the CuO NPs surface . The weights of (0.0300 g)and (0.0100 g) gave the best removal percentage for CR and SA dyes, respectively, so they were used in subsequent experiments .

Table 3.2 Effect of adsorbent dose on adsorption of CR and SA dyes on CuONPs at 298 K.

Wt. (g)	Removal %= $\frac{C_0 - C_e}{C_0} \times 100$	
	Congo Red	**Safranin**
0.0050	96.4061	94.8856
0.0100	96.5858	**95.6879**
0.0200	96.7655	95.2868
0.0300	97.2147	95.3870
0.0400	97.1248	95.4873
0.0500	97.0350	95.4873
0.0600	97.0350	95.5876
0.0700	97.1248	95.5876
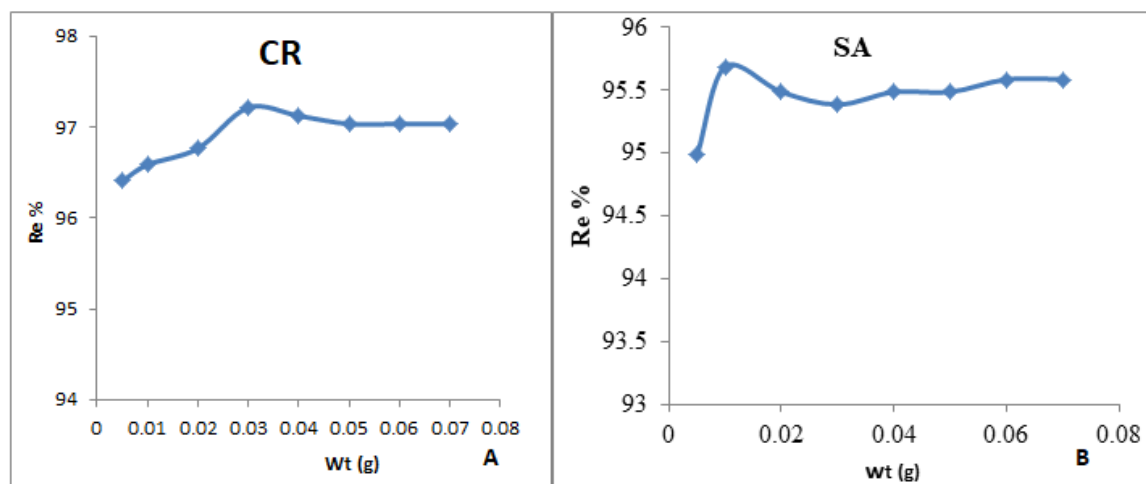
Figure 3.7 Effect of adsorbent dose on adsorption of CR and SA dyes on CuONPs at 298 K.

3.2.3- Effect of pH

The removal of CR and SA dyes on the surface of the CuONPs was studied in acidic functions within the range of (3,5,7,9 and 11).The concentrations of CR and SA dyes were (35.0000mg/L) and (12.0000mg/L), respectively, at 298K. The study's findings are shown in Figure 3.8 and Table 3.3 .

Table 3.3 Effect of pH on adsorption of CR and SA dyes on CuONPs at 298K.

pH	Removal %= $\frac{C_0-C_e}{C_0} \times 100$	
	Congo Red	**Safranin**
3	**98.2929**	82.0497
5	97.9335	95.1865
7	97.3045	95.8884
9	95.8670	96.2896
11	95.7771	96.0890
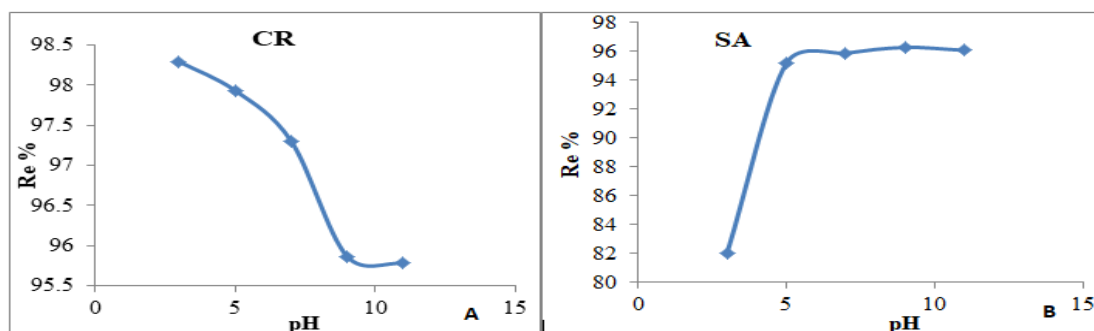
Figure 3.8 Effect of pH on adsorption of CR and SA dyes on CuONPs at 298 K.

The results show that the amount of adsorption of the CR dye on the surface of CuO NPs increases in the acid medium, in contrast, decreases in the basic medium, where the acid function of CR was pH=3. The values were adopted for further optimizations , with the percentage of removal being 98.2929, while for the SA dye acid function was at pH = 9, and the rate of removal was 96.2896. These values were adopted as acid functions for adsorption systems .

3.2.4 - Effect of ionic strength

The effect of ionic strength on adsorption capacity and removal percentage was studied by using different concentrations ranging between (0.0200-0.0700 M) of salts (NaCl , KCl, $MgCl_2$ and $CaCl_2$), with concentrations of 35.0000 mg/L and 12.000 mg/L of Congo Red and Safranin-O dyes were used, respectively. It was found that adsorption capacity decreased as ionic strength went up. This may be because the dye is more soluble than the salt used to raise ionic strength [128] . Consequently, this characteristic makes it competitive with ions. The salts employed to connect with the surface are more than the dye, thereby decreasing the surface's absorption capacity. The findings of the investigation also revealed that the impact of the various salts on the charge and size of the two dyes varied. Figures 3.9 show As demonstrated in Figures 3.9

and Table 3.4, the tiny size and small charge provide a very obvious ratio for the removal of both dyes due to their small size and charge .

Table 3.4 Effect of ionic strength on adsorption a (CR) and b (SA) at 298K.

	molar concentration of salt (M)	Removal percentage R%			
		NaCl	KCl	MgCl$_2$	CaCl$_2$
CR	0.02	98.1132	97.9335	97.7538	97.5741
	0.05	98.0233	97.8436	97.6639	97.4842
	0.07	97.9335	97.7538	97.5741	97.3944
SA	0.02	78.8407	76.8351	74.3281	68.7123
	0.05	70.8182	68.6121	63.7986	61.1913
	0.07	68.7123	65.0020	61.8933	58.8848
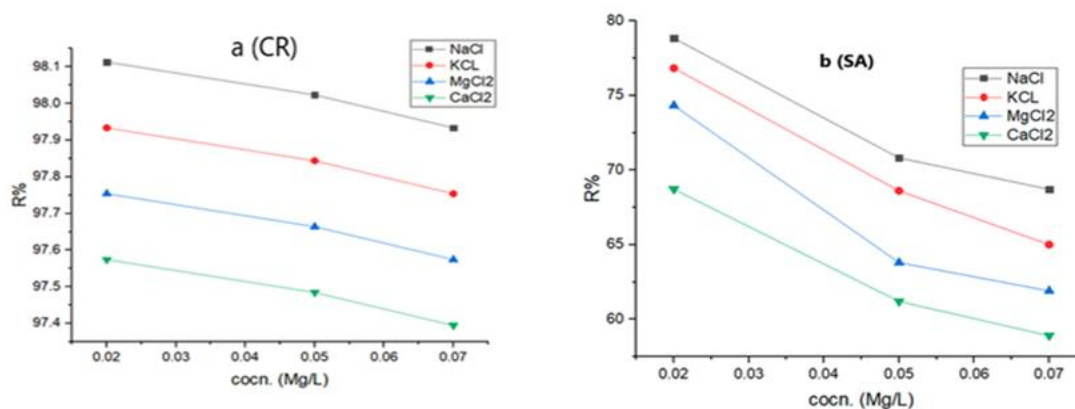
Figure 3.9 Effect of ionic strength on adsorption a (CR) and b (SA) at 298 K.

3.2.5 -Effect of temperature

The effect of temperature on the adsorption extent of CR and SA dyes on CuO NPs was studied at different temperatures (288, 298 , 308 , and 318 K). The results of this study are depicted in Figure 3.10 and Table 3.5. The results indicated a decrease in the amount of CR and SA dyes that are adsorbed on

CuO NPs with an increase in temperature; hence, the adsorption process appears to be exothermic for CR dye and endothermic for SA dye [129].

The study of temperature effect on adsorption of CR and SA on CuO NPs surfaces would help in evaluating the basic thermodynamic functions, the Gibbs energy(ΔG), the enthalpy (ΔH) and the entropy (ΔS) of the adsorption process[130] .

$$\textbf{keq} = \frac{Q_e\ M}{C_0\ V} \ \ldots\ldots\ldots. \ \textbf{(3-2)}$$

(Keq) = Each temperature's equilibrium constant for the adsorption process.
V = the volume of the solution (L) .
 M = the adsorbent mass (g) .

$$\Delta G = -RT \ln k_{eq} \ \ldots\ldots..(3\text{-}3)$$

ΔG = Gibbs energy (J/mol)
 R = the ideal gas constant (8.314 J/mol. K)
 T = the absolute temperature (K)
Table(3.5) gives K_{eq} values at different temperatures

The heat of adsorption (ΔH) may be obtained from Van't Hoff equation[131]

$$\textbf{ln keq} = -\frac{\Delta H}{R\,T} + \textbf{Constant} \ \ \ldots\ldots\ldots(3\text{-}4)$$

The relationship (lnKeq vs. 1/T)) result in a straight line with slope =(- ΔH / R)
As seen in Figure 3.10

The entropy change (ΔS) was calculated from Gibbs- Helmholtz equation

$$\Delta G = \Delta H - T\Delta S \ \ldots\ldots\ldots\ldots\ldots \ \textbf{(3-5)}$$

ΔS = Entropy (J mol^{-1})
ΔH = Enthalpy (KJ mol^{-1})

Table 3.6 show the thermodynamic functions ΔG,ΔH and ΔS and for the removal of CR and SA dyes on CuO NPs respectively at different temperatures.

Table 3.5 Equilibrium constant values CuONPs at different temperatures .

ln k_{eq} CR	ln k_{eq} SA	T(K)	1/T (K^{-1})
4.3630	2.8030	288	0.0034
4.0531	2.9844	298	0.0033
3.7330	3.1493	308	0.0032
3.4574	3.2846	318	0.0031
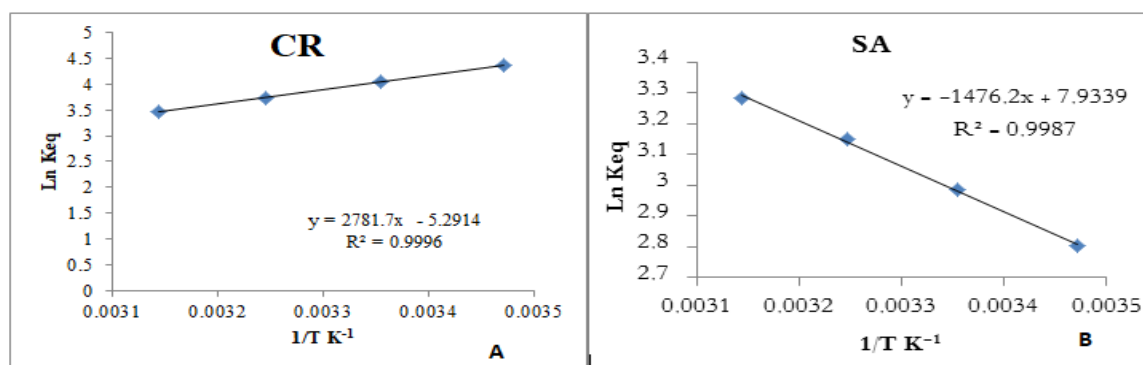
Figure 3.10 Plot ln K$_{eq}$ versus 1/T of CR and SA dyes on the adsorption surfaces for CuONPs.

Table 3.6 . Thermodynamic function ΔG, ΔH and ΔS of CR and SA on the adsorbent surface CuO NPs at different temperatures

Adsorbate	Temp.	ΔG (kJ/mol)	ΔH (kJ/mol)	ΔS (kJ/mol.K)
CR	288 K	-10.4470		- 0.0440
	298 K	-10.0421		- 0.0439
	308 K	-9.5593	-23.1271	- 0.0440
	318 K	- 9.1409		- 0.0439
SA	288 K	- 6.7116		0.0659
	298 K	- 7.3941		0.0659
	308K	- 8.0646	12.2731	0.0660
	318 K	- 8.6841		0.0659

The ΔG values are found to be negative at all tested temperatures (288, 298,298 ,308 and 318 K), indicating that the adsorption of CR and SA dyes on the adsorbent surfaces (CuO NPs) is spontaneous and thermodynamically favorable. ΔH values that are negative imply that the adsorption of CR dye using surface CuONPs has been an exothermic ,ΔH values that are positive imply that the adsorption of SA dye using surface CuONPs has been an endothermic process. ΔS for CR is the negative because the dye is symmetrical, the adsorption is stronger on either side. The values of ΔS for both dyes are very small and refer to a decrease in randomness, which means good adsorption happened (randomness of adsorbed molecules with adsorption) the difference in signal is due to symmetry in Congo red structural [132].The adsorption process in

the solid–liquid system is a combination of two processes: (a) the desorption of the solvent (water) molecules previously adsorbed, and (b) the adsorption of the adsorbate species. In an endothermic process, the adsorbate species has to displace more than one water molecule for their adsorption and this result in the endothermicity of the adsorption process.Therefore ΔH will be positive. In an exothermic process, the total energy absorbed in bond breaking is less than the total energy released in bond making between adsorbate and adsorbent, resulting in the release of extra energy in the form of heat. Therefore ΔH will be negative. The magnitude of ΔH may also give an idea about the type of sorption. The heat evolved during physical adsorption is of the same order of magnitude as the heats of condensation, i.e., 2.1–20.9 kJ mol^{-1}, while the heats of chemisorption generallyfalls into a range of 80–200 kJ mol^{-1}. [133]

3.3 Adsorption isotherms

The general shape of the CR and SA dyes adsorption isotherm on the CuONPs are shown in Figures 3.11 and 3.12 and Table 3.7,where the quantities of adsorbed on CuONPs (Qe) are plotted a function of equilibrium concentration (Ce) at (288 ,298,308 and 318 K). The shape of the adsorption isotherms of CR and SA dyes on the two CuONPs is in consistent with (4S-type) on the Giles classification [74]. In the adsorption of dyes such as CR and SA dyes on CuONPs surfaces, there is an electrostatic attraction between the surface or crystal structure of the CuONPs which are negatively charge, and the

positively charge dye ion. Therefore, an isotherm of (4S-type) is expected and in this case has a high probability to behave like an ion exchange. According to Giles interpretation for the adsorption isotherm shape, the CR and SA dyes could be oriented in a direction which is parallel to the surface of CuONPs [134] .

Table 3.7 The adsorption values of congo red and safranin-O dyes on the surface of CuONPs at different temperatures.

Temp.		288 K			298K		308K		318K	
Adsorbate	Co (mg/L)	Ce (mg/L)	Qe (mg/g)	Ce (mg/L)	Qe (mg/g)	Ce (mg/L)	Qe (mg/g)	Ce (mg/L)	Qe (mg/g)
CR	5	0.0314	4.1404	0.0628	4.1142	0.0943	4.0880	0.1257	4.0618
	10	0.0943	8.2547	0.1257	8.2285	0.1886	8.1761	0.2515	8.1236
	15	0.1572	12.3691	0.2201	12.316	0.3144	12.2379	0.3773	12.1855
	20	0.2201	16.4832	0.3144	16.4046	0.4402	16.2997	0.5345	16.2211
	25	0.2830	20.5975	0.4088	20.4926	0.5660	20.3616	0.6918	20.2568
	30	0.3459	24.7117	0.5031	24.5807	0.6918	24.4234	0.8490	24.2924
	35	0.4402	28.7998	0.5974	28.6687	0.8176	28.4853	1.0691	28.2756
	40	0.5345	32.8878	0.7232	32.7306	0.9433	32.5471	1.2264	32.3113
	45	0.6289	36.9759	0.9119	36.7400	1.1635	36.5304	1.4150	36.3207
	50	0.7861	41.0115	1.0377	40.8018	1.3207	40.5660	1.5723	40.3563
	55	0.8805	45.0995	1.1635	44.8637	1.4779	44.6016	1.7610	44.3658
SA	2.5	0.2286	5.6784	0.2045	5.73856	0.1564	5.8589	0.1203	5.9491
	5	0.3489	11.6275	0.3249	11.6877	0.2406	11.8983	0.1925	12.0186
	7	0.42117	16.4470	0.3730	16.5673	0.3369	16.6576	0.2527	16.8682
	9	0.5535	21.1161	0.4452	21.3868	0.3971	21.5072	0.3489	21.6275
	10	0.6137	23.4657	0.5174	23.7063	0.4572	23.8568	0.3730	24.0673
	12	0.6859	28.2852	0.5776	28.5559	0.4933	28.7665	0.4332	28.9169
	15	0.7340	35.6648	0.6257	35.9356	0.5535	36.1161	0.4693	36.3267
	18	0.7821	43.0445	0.6859	43.2852	0.6016	43.4957	0.5174	43.7063
	21	0.8303	50.4241	0.7460	50.6347	0.6498	50.8754	0.5655	51.0860
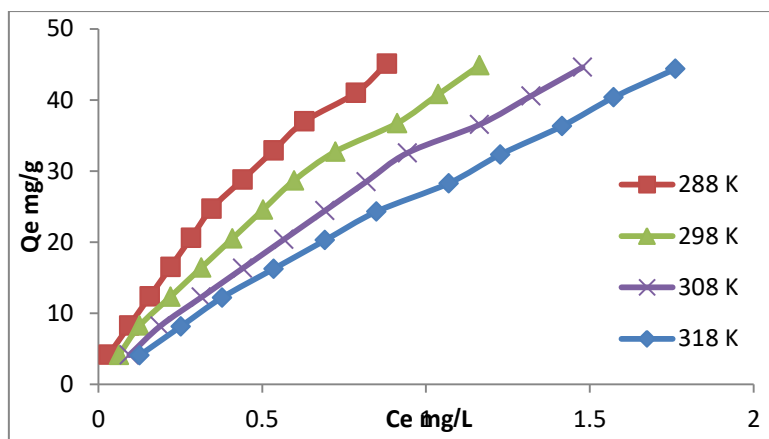
Figure 3.11 . Adsorption isotherm for congo red dye from aqueous solution using 0.0300 g from surface the CuO NPs at different temperatures .
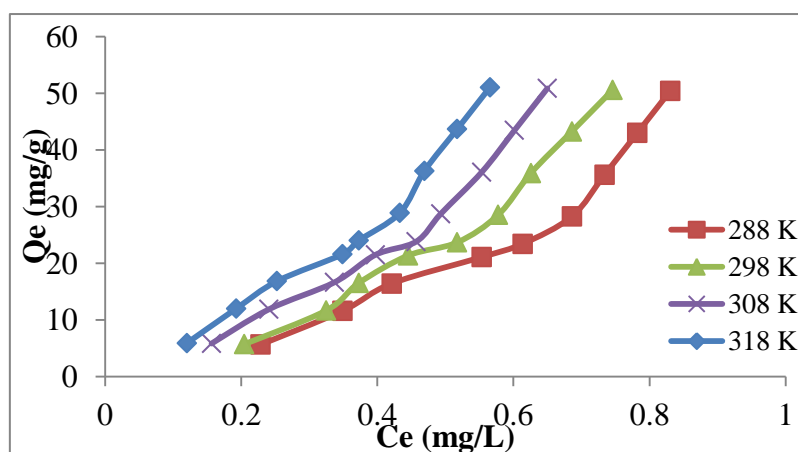
Figure 3.12 . Adsorption isotherm for safranin-O dye from aqueous solution using 0.0100 g from surface the CuONPs at different temperatures.

3.4 Adsorption isotherm models

The experiment equilibrium adsorption data were analyzed using Langmuir , Freundlich , Temkin and Halsey adsorption isotherm models .

3.4.1 Langmuir isotherm model

The Langmuir isotherm is represented by the equation (1.1) The linear plots of C_e/Q_e versus C_e suggest the applicability of the Langmuir isotherms as shown in Table 3.8. The values of a ,b and R_L were determined from the slope and intercept of the plot shows in Figures 3.13 and Tables (3.12 and 3.13) . This isotherm is less fitting than the Freundlich, Temkin, and Halsey isotherms,

which means the results indicate multi-layer adsorption. R_L value indicates the adsorption nature to be either favourable (0 R_L 1), unfavourable ($R_L < 1$), linear ($R_L = 1$) or irreversible ($R_L = 0$) [61]

Table 3.8 Langmuir data of adsorption CR and SA dyes on CuO NPs at different temperatures .

Temp.	288K		298K		308K		318K	
Adsorb	Ce (mg/L)	Ce/Qe (g/L)	Ce (mg/L)	Ce/Qe (g/L)	Ce (mg/L)	Ce/Qe (g/L)	Ce (mg/L)	Ce/Qe (mg/g)
CR	0.0314	0.0075	0.0628	0.0152	0.0943	0.0230	0.1257	0.0309
	0.0943	0.0114	0.1257	0.0152	0.1886	0.0230	0.2515	0.0309
	0.1572	0.0127	0.2201	0.0178	0.3144	0.0256	0.3773	0.0309
	0.2201	0.0133	0.3144	0.0191	0.4402	0.0270	0.5345	0.0329
	0.2830	0.0137	0.4088	0.0199	0.5660	0.0277	0.6918	0.0341
	0.3459	0.0139	0.5031	0.0204	0.6918	0.0283	0.8490	0.0349
	0.4402	0.0152	0.5974	0.0208	0.8176	0.0287	1.0691	0.0378
	0.5345	0.0162	0.7232	0.0220	0.9433	0.0289	1.2264	0.0379
	0.6289	0.0170	0.9119	0.0248	1.1635	0.0318	1.4150	0.0389
SA	0.2286	0.0402	0.2045	0.0356	0.1564	0.0267	0.1203	0.0202
	0.3489	0.0300	0.3249	0.0277	0.2406	0.0202	0.1925	0.0160
	0.4211	0.0256	0.3730	0.0225	0.3369	0.0202	0.2527	0.0149
	0.5535	0.0262	0.4452	0.0208	0.3971	0.0184	0.3489	0.0161
	0.6137	0.0261	0.5174	0.0218	0.4572	0.0191	0.3730	0.0155
	0.6859	0.0242	0.5776	0.0202	0.4933	0.0171	0.4332	0.0149
	0.7340	0.0205	0.6257	0.0174	0.5535	0.0153	0.4693	0.0129
	0.7821	0.0181	0.6859	0.0158	0.6016	0.0138	0.5174	0.0118
	0.8303	0.0164	0.7460	0.0147	0.6498	0.0127	0.5655	0.0110
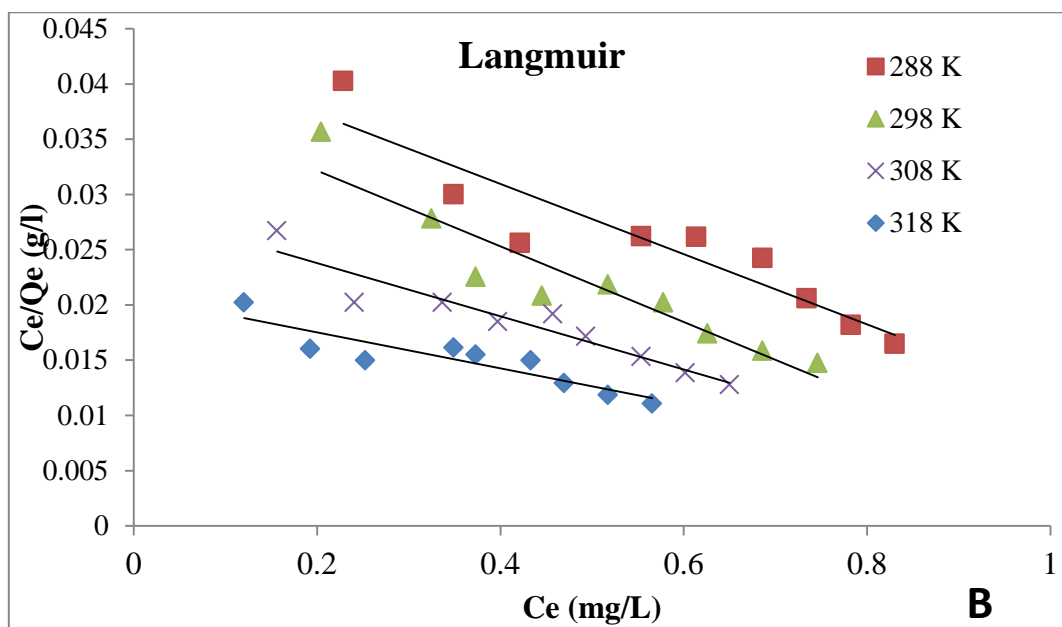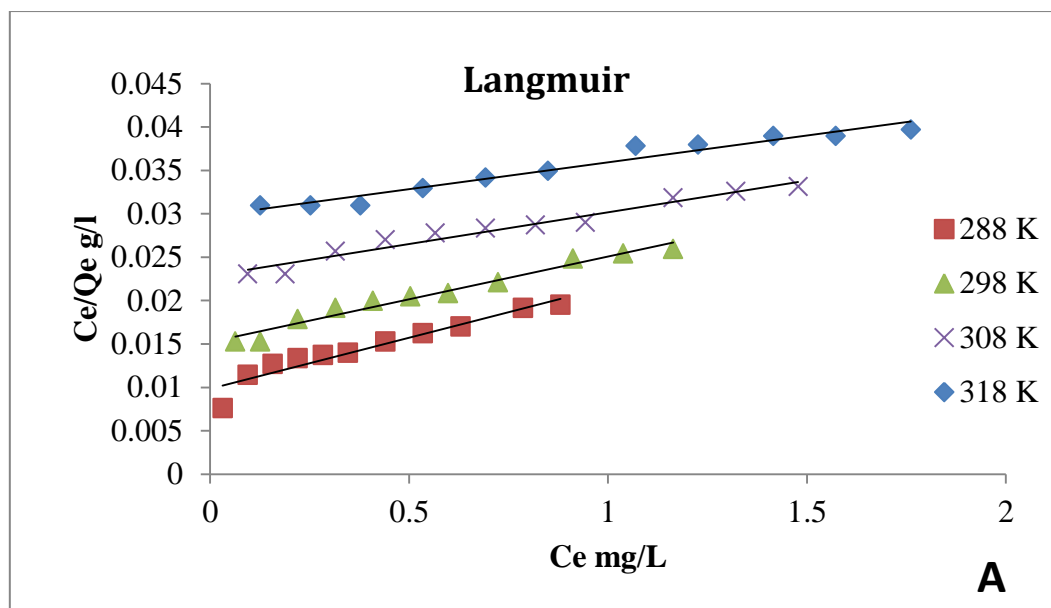
**Figure 3.13 Langmuir isotherms model of adsorption of(A) congo red and (B)
safranin-O dyes on CuONPs at different temperatures**

3.4.2 Freundlich isotherm model

Freundlich adsorption isotherm model used to explain the adsorption
phenomenon is represented by equation(1.4).Linear plot of $\log Q_e$
versus $\log C_e$ shows that the adsorption CR) and (SA) dyes follows the
Freundlich isotherm figures (3.14) and tables (3.9) . The values of K_F
and n were calculated from the intercept and slope of the plot. The
magnitude of the exponent (n) gives an indication of the favourability

and K_F the capacity of the adsorbent/adsorbate. The values of 1/n , less than unity represent favourable adsorption and values of 1/n>1 indicate unfavourable adsorption. The results for CR and SA dyes adsorption systems of this study are favourable show in Tables (3.12) and (3.13) .

Table 3.9. Freundlich data of adsorption CR and SA dyes on CuO NPs at different temperatures .

| Temp.	288 K		298 K		308 K		318 K	
Adsorbate	Log Ce	Log Qe	Log Ce	Log Qe	Log Ce	Log Qe	Log Ce	Log Qe
CR	-1.5024	0.6170	-1.2014	0.6142	-1.0253	0.6115	-0.9003	0.6087
	-1.0253	0.9167	-0.9003	0.9153	-0.7242	0.9125	-0.5993	0.9097
	-0.8034	1.0923	-0.6573	1.0904	-0.5024	1.0877	-0.4232	1.0858
	-0.6573	1.2170	-0.5024	1.2149	-0.3563	1.2121	-0.2719	1.2100
	-0.5481	1.3138	-0.3884	1.3115	-0.2471	1.3088	-0.1602	1.3065
	-0.4610	1.3929	-0.2983	1.3905	-0.1602	1.3878	-0.0710	1.3854
	-0.3563	1.4593	-0.2236	1.4574	-0.0874	1.4546	0.0290	1.4514
	-0.2719	1.5170	-0.1407	1.5149	-0.0253	1.5125	0.0886	1.5093
	-0.2014	1.5679	-0.0400	1.5651	0.0657	1.5626	0.1507	1.5601
	-0.1044	1.6129	0.01608	1.6106	0.1208	1.6081	0.1965	1.6059
	-0.0552	1.6541	0.06577	1.6518	0.1696	1.6493	0.2457	1.6470
SA	-0.6408	0.7542	-0.6891	0.7588	-0.8056	0.7678	-0.9196	0.7744
	-0.4572	1.0654	-0.4882	1.0677	-0.6185	1.0754	-0.7154	1.0798
	-0.3755	1.2160	-0.4282	1.2192	-0.4724	1.2216	-0.5973	1.2270
	-0.2568	1.3246	-0.3514	1.3301	-0.4010	1.3325	-0.4572	1.3350
	-0.2120	1.3704	-0.2861	1.3748	-0.3398	1.3776	-0.4282	1.3814
	-0.1637	1.4515	-0.2383	1.4556	-0.3068	1.4588	-0.3633	1.4611
	-0.1342	1.5522	-0.2036	1.5555	-0.2568	1.5577	-0.3285	1.5602
	-0.1066	1.6339	-0.1637	1.6363	-0.2206	1.6384	-0.2861	1.6405
	-0.0807	1.7026	-0.1272	1.7044	-0.1872	1.7065	-0.2475	1.7083
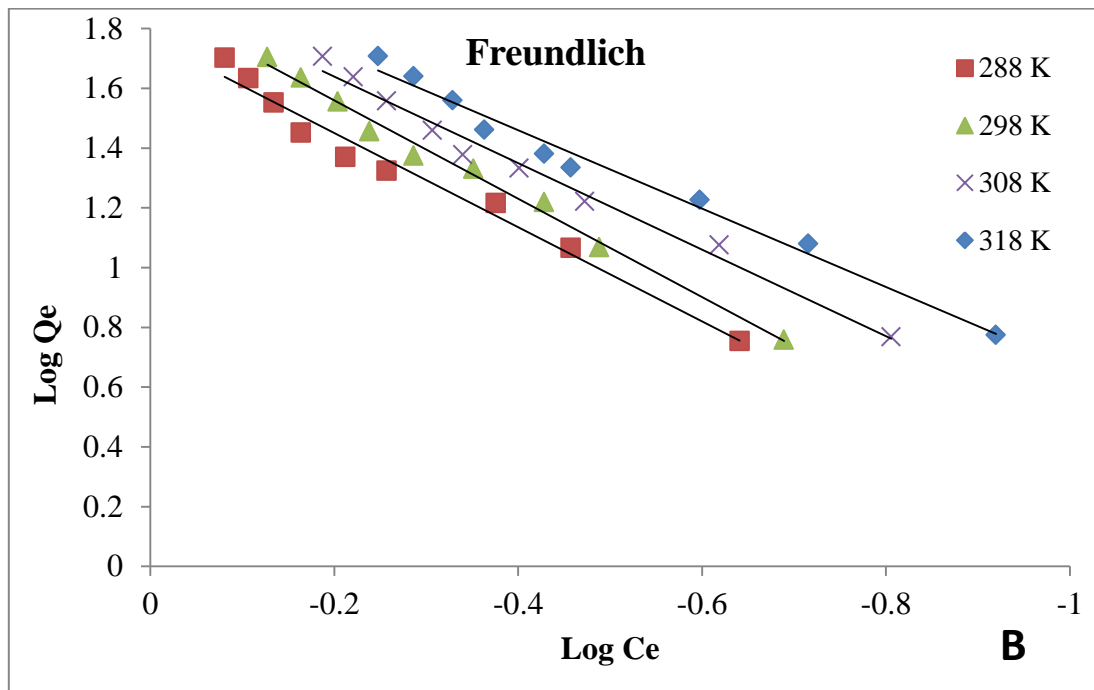
Figure 3.14 Freundlich isotherms model of adsorption of(A) congo red and (B) safranin-O dyes on CuONPs at different temperatures

3.4.3 Temkin isotherm model

Temkin isotherm equation (1.5) was used to figure out the adsorption isotherm of CuO NPs at different temperatures. Table (3.10) and Figure (3.15) show adsorption isotherm data for (CR) and (SA) dyes.The Temkin isotherm constants (A_T) and (B are proportional to the adsorption heat, calculated from the intercept and slope of the plotas of (Q_e)versus $\ln C_e$ and the results are shown in Tables (3.12) and (3.13) .

Table 3.10 Temkin data of adsorption CR and SA dyes on CuO NPs at different temperatures .

| Temp.K	288 K		298 K		308 K		318 K	
Adsorbate	ln Ce	Qe	ln Ce	Qe	ln Ce	Qe	ln Ce	Qe
CR	-3.4594	4.14046	-2.7663	4.1142	-2.3608	4.0880	-2.0731	4.0618
	-2.3608	8.25471	-2.0731	8.2285	-1.6677	8.1761	-1.3800	8.1236
	-1.8500	12.3689	-1.5135	12.3165	-1.1568	12.237	-0.9745	12.1855
	-1.5135	16.4832	-1.1568	16.4046	-0.8204	16.2997	-0.6262	16.2211
	-1.2622	20.5974	-0.8945	20.4926	-0.5690	20.3616	-0.3684	20.2568
	-1.0615	24.7117	-0.6868	24.5807	-0.3684	24.4234	-0.1636	24.2924
	-0.8204	28.7997	-0.5150	28.6687	-0.2013	28.4853	0.0668	28.2756
	-0.6262	32.8878	-0.3239	32.7306	-0.0582	32.5471	0.2040	32.3113
	-0.4637	36.9758	-0.0921	36.7400	0.1514	36.5304	0.3471	36.3207
	-0.2405	41.0115	0.0370	40.8018	0.2782	40.5660	0.4525	40.3563
	-0.1272	45.0995	0.1514	44.8637	0.3906	44.6016	0.5658	44.3658
SA	-1.4756	5.6784	-1.5868	5.7385	-1.8551	5.8589	-2.1174	5.9491
	-1.0527	11.6275	-1.1242	11.6877	-1.4243	11.8983	-1.6474	12.0186
	-0.8647	16.4470	-0.9860	16.5673	-1.0878	16.6576	-1.3755	16.8682
	-0.5914	21.1161	-0.8091	21.3868	-0.9235	21.5072	-1.0527	21.6275
	-0.4882	23.4657	-0.6588	23.7063	-0.7824	23.8568	-0.9860	24.0673
	-0.3769	28.2852	-0.5488	28.5559	-0.7064	28.7665	-0.8365	28.9169
	-0.3091	35.6648	-0.4688	35.9356	-0.5914	36.1161	-0.7564	36.3267
	-0.2456	43.0445	-0.3769	43.2852	-0.5080	43.4957	-0.6588	43.7063
	-0.1859	50.4241	-0.2929	50.6347	-0.4310	50.8754	-0.5699	51.0860

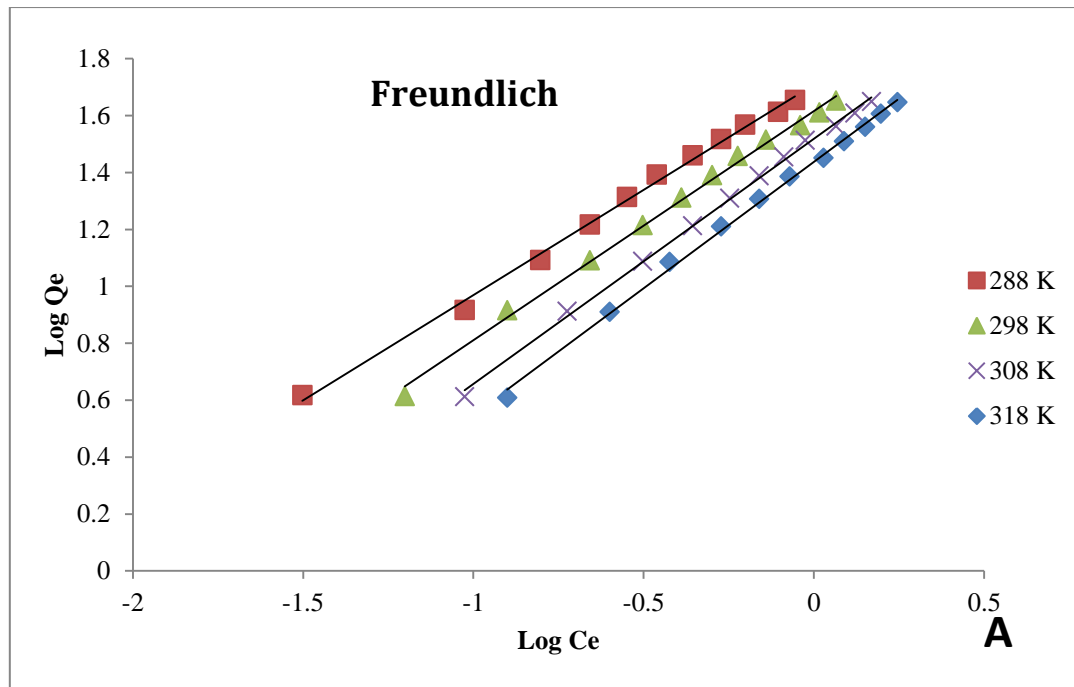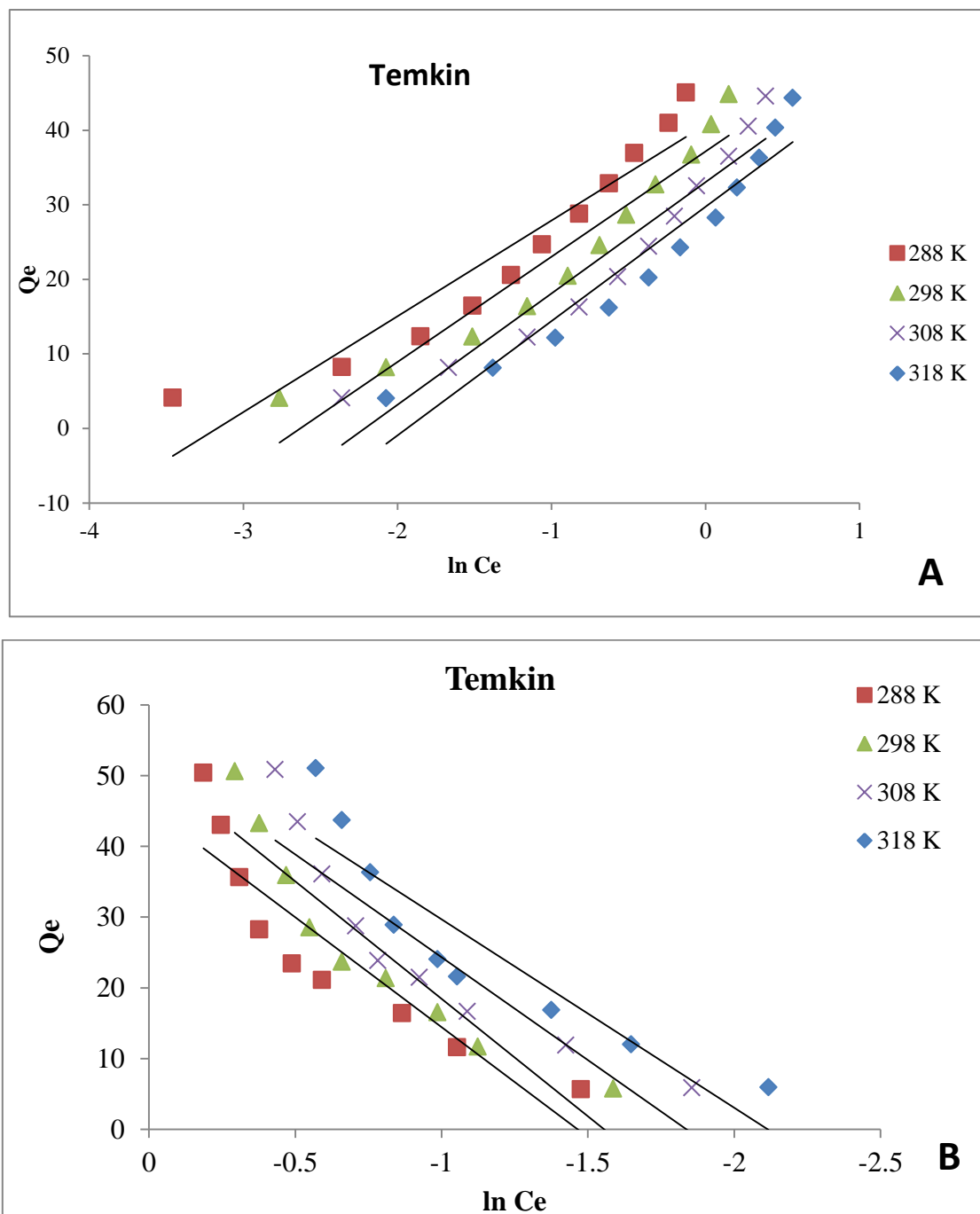**Figure 3.15 Temkin isotherms model of adsorption of(A) congo red and (B) safranin-O dyes on CuONPs at different temperatures**

3.4.4 <u>Halsey isotherm model</u>

The Halsey adsorption isotherm model used to explain the adsorption phenomenon is represented by equation (1.7). The (CR) and (SA) dyes' adsorption isotherm data were plotted and displayed in a table (3.11). Halsey isotherm constants (K_H) and (n_H) are calculated from the slope and intercept the plots of $\ln Q_e$ versus $\ln (C_e)$ and the results are shown in Figure(3.16). In Tables (3.12) and (3.13), .

Table 3.11 Halsey data of adsorption CR and SA dyes on CuO NPs at different temperatures .

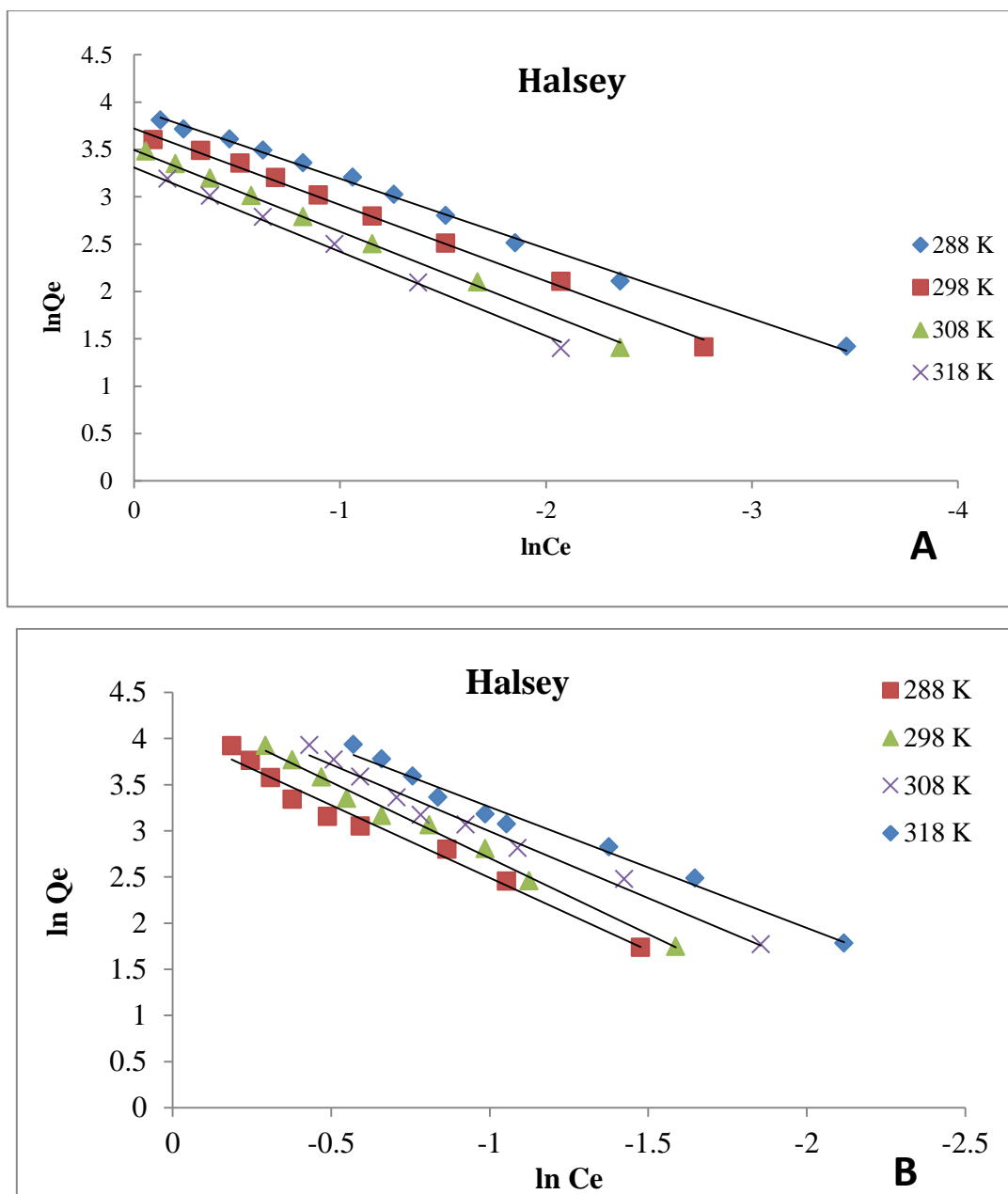| Temp.K	288 K		298 K		308 K		318 K	
Adsorbate	ln Ce	lnQe	ln Ce	lnQe	ln Ce	lnQe	ln Ce	lnQe
CR	-1.4756	1.7366	-1.5868	1.7472	-1.8551	1.7679	-2.1174	1.7832
	-1.0527	2.4533	-1.1242	2.4585	-1.4243	2.4763	-1.6474	2.4864
	-0.8647	2.8001	-0.9860	2.8074	-1.0878	2.8128	-1.3755	2.8254
	-0.5914	3.0500	-0.8091	3.0627	-0.9235	3.0683	-1.0527	3.0739
	-0.4882	3.1555	-0.6588	3.1657	-0.7824	3.1720	-0.9860	3.1808
	-0.3769	3.3423	-0.5488	3.3518	-0.7064	3.3592	-0.8365	3.3644
	-0.3091	3.5741	-0.4688	3.5817	-0.5914	3.5867	-0.7564	3.5925
	-0.2456	3.7622	-0.3769	3.7678	-0.5080	3.7726	-0.6588	3.7774
	-0.1859	3.9204	-0.2929	3.9246	-0.4310	3.9293	-0.5699	3.9335
	-1.4756	1.7366	-1.5868	1.7472	-1.8551	1.7679	-2.1174	1.7832
	-1.0527	2.4533	-1.1242	2.4585	-1.4243	2.4763	-1.6474	2.4864
SA	-1.4756	1.7366	-1.5868	1.7472	-1.8551	1.7679	-2.1174	1.7832
	-1.0527	2.4533	-1.1242	2.4585	-1.4243	2.4763	-1.6474	2.4864
	-0.8647	2.8001	-0.9860	2.8074	-1.0878	2.8128	-1.3755	2.8254
	-0.5914	3.0500	-0.8091	3.0627	-0.9235	3.0683	-1.0527	3.0739
	-0.4882	3.1555	-0.6588	3.1657	-0.7824	3.1720	-0.9860	3.1808
	-0.3769	3.3423	-0.5488	3.3518	-0.7064	3.3592	-0.8365	3.3644
	-0.3091	3.5741	-0.4688	3.5817	-0.5914	3.5867	-0.7564	3.5925
	-0.2456	3.7622	-0.3769	3.7678	-0.5080	3.7726	-0.6588	3.7774
	-0.1859	3.9204	-0.2929	3.9246	-0.4310	3.9293	-0.5699	3.9335

Figure 3.16. Halsey isotherms model of adsorption of(A) congo red and (B) safranin-O dyes on CuONPs at different temperatures

Table 3.12 Langmuir, Freundlich , Temkin and Halsey parameters of adsorption isotherms of congo red dye on CuO NPs at different temperatures.

Temp.(K)	Langmuir isotherm				Freundlich isotherm		
	-a(mg/g)	-b(mg/L)	-R_L	R^2	K_F	n	R^2
288K	84.7457	1.2040	0.0243	O.9171	51.0387	1.3529	0.9965
298K	101.0101	0.6513	0.0458	0.9692	41.3142	1.2416	0.9965
308K	136.9863	0.3187	0.0984	0.9604	32.9382	1.1611	0.9981
318K	161.2903	0.2080	0.1591	0.9556	27.3275	1.1265	0.9978
Temp.(K)	Temkin isotherm			Halsey isotherm		
	B	A_T	R^2	n_H	K_H	R^2
288K	12.853	23.86495	0.8994	1.3529	204.5065	0.9965
298K	14.132	13.88048	0.9258	1.2416	101.5245	0.9965
308K	14.947	9.13533	0.9182	1.1611	57.85269	0.9981
318K	15.349	6.95237	0.9215	1.1265	41.52933	0.9978

From the results the (R^2) values in the table (3.12) for Langmuir, Freundlich , Temkin and Halsey (Physisorption), it turns out that the best results are in the Freundlich and Halsey values [75, 79, 81, 83] .

Table 3.13 Langmuir, Freundlich , Temkin and Halsey parameters of adsorption isotherms of safranin-O dye on CuO NPs at different temperatures.

Temp.(K)	Langmuir isotherm				Freundlich isotherm		
	-a(mg/g)	-b(mg/L)	-R_L	R^2	K_H	n	R^2
288K	31.446	0.727	O.129	O.8647	58.411	0.634	0.9777
298K	29.239	0.876	0.105	0.8846	77.41	0.607	0.9910
308K	41.666	0.839	0.11	0.9044	84.937	0.69	0.9857
318K	62.893	0.764	0.122	0.7508	96.671	0.761	0.9832
Temp.(K)	Temkin isotherm			Halsey isotherm		
	B	A_T	R^2	n_H	K_H	R^2
288K	31.05	4.325	0.8278	0.634	609.56	0.9777
298K	33.22	4.738	0.8715	0.607	1282.82	0.9910
308K	29.07	6.276	0.8403	0.69	620.8	0.9857
318K	26.64	8.283	0.844	0.761	403.42	0.9832

According to (R^2) values in the table (3.13) for Langmuir, Freundlich ,Temkin and Halsey(Chemisorption) it can be concluded that the best results are in the Freundlich and Halsey values.

3.5 Hemolysis activity

CuONPs derived from (*Anchusa strigosa L*). were evaluated against normal human erythrocytes for their hemolysis activity. CuONPs had a negligible impact on blood hemolysis when compared to negative and positive controls. Figure 3.17 depicts the hemolisis activity of the CuONPs as a percentage of hemolysis for 60 healthy, non-smoking donors .
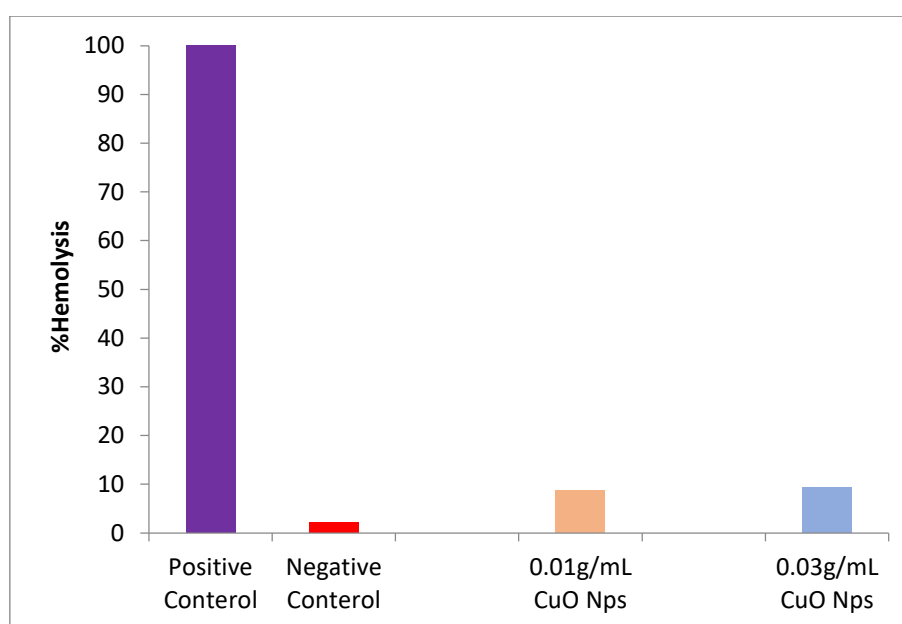
Figure 3.17   The proportion of hemolysis that CuONPs generate. Positive control was triton X-100 and negative control was normal saline.

Using bioactive chemicals derived from herbs and medicinal plants may influence the erythrocyte membrane. Concentration increases have exacerbated the hemolytic impact [135]. When red blood cells come into contact with water, hemolysis occurs; thus, the implant material must be properly inspected before use [136]. Prior research on CuONPs has shown that smaller particles had more hemolytic activity than larger particles; however, for silica nanoparticles, the hemolytic activity increased as the particle size increased

[137]. During medication design, the toxicity of the active molecule is a crucial factor to consider, and hemolysis activity is a good place to begin since it gives fundamental information on the interactions between molecules and biological entities at the cellular level. Hemolysis activity indicates broad cytotoxicity toward healthy, normal cells. The spectroscopic in vitro hemolysis test is a straightforward and effective method for quantifying hemolysis. This approach measures the impact of various biomolecule concentrations on human erythrocytes [110] .

Table (3-14). The percentage of hemolysis induced by copper oxide, and absorbance for blood with CuO NPs (0.01 g/mL) , with normal saline, and with D.W. Hemolysis % with positive control 100% .

Abs with CuONPs(0.01 g/mL)	Abs with normal saline	Abs with D.W.	Hemolysis %
0.058	0.032	0.365	7.8078
0.072	0.051	0.524	4.4397
0.078	0.055	0.51	5.0549
0.095	0.066	0.556	5.9183
0.104	0.075	0.575	5.8008
0.106	0.092	0.528	3.2110
0.122	0.101	0.636	3.9252
0.128	0.116	0.639	2.2944
0.13	0.111	0.651	3.5185
0.157	0.091	0.669	11.4186
0.175	0.122	0.636	10.3112
0.21	0.125	0.856	11.6279
0.058	0.022	0.315	7.8078
0.072	0.055	0.724	4.4397
0.078	0.057	0.501	5.0549
0.095	0.061	0.454	5.9183

0.104	0.065	0.371	5.8008
0.106	0.082	0.566	3.2110
0.122	0.111	0.642	3.9252
0.128	0.126	0.641	2.2944
0.13	0.121	0.681	3.5185
0.157	0.031	0.717	11.4186
0.175	0.022	0.636	10.3112
0.21	0.152	0.756	11.6279
0.058	0.042	0.465	7.8078
0.072	0.081	0.324	4.4397
0.078	0.045	0.451	5.0549
0.095	0.076	0.656	5.9183
0.104	0.045	0.787	5.8008
0.106	0.052	0.468	3.2110
0.122	0.091	0.636	3.9252
0.128	0.106	0.652	2.2944
0.13	0.071	0.611	3.5185
0.157	0.041	0.539	11.4186
0.175	0.082	0.716	10.3112
0.21	0.125	0.856	11.6279
0.058	0.112	0.495	7.8078
0.072	0.071	0.524	4.4397
0.078	0.095	0.651	5.0549
0.095	0.076	0.446	5.9183
0.104	0.035	0.675	5.8008
0.106	0.072	0.428	3.2110
0.122	0.161	0.736	3.9252
0.128	0.056	0.642	2.2944
0.13	0.111	0.451	3.5185
0.157	0.091	0.621	11.4186

0.175	0.102	0.536	10.3112
0.21	0.065	0.751	11.6279
0.058	0.032	0.856	7.8078
0.072	0.101	0.441	4.4397
0.078	0.115	0.224	5.0549
0.095	0.106	0.660	5.9183
0.104	0.085	0.532	5.8008
0.106	0.062	0.712	3.2110
0.122	0.101	0.528	3.9252
0.128	0.103	0.717	2.2944
0.13	0.117	0.801	3.5185
0.157	0.091	0.398	11.4186
0.175	0.120	0.801	10.3112
0.21	0.125	0.801	11.6279
Average			6.1744

Table (3-15). The percentage of hemolysis induced by copper oxide, and absorbance for blood with CuO NPs (0.03 g/mL) , with normal saline, and with D.W. with positive control 100% .

Abs with CuONPs(0.03 g/mL)	Abs with normal saline	Abs with D.W.	Hemolysis %
0.077	0.032	0.365	13.5135
0.081	0.051	0.524	6.3424
0.097	0.055	0.51	9.2307
0.125	0.066	0.556	12.0408
0.13	0.075	0.575	11.6541
0.133	0.092	0.528	9.40367
0.139	0.101	0.636	7.10280

0.142	0.116	0.639	4.9713
0.146	0.111	0.651	6.4814
0.155	0.091	0.669	11.0726
0.174	0.122	0.636	10.1167
0.193	0.125	0.856	9.3023
0.077	0.022	0.315	13.5135
0.081	0.055	0.724	6.3424
0.097	0.057	0.501	9.2307
0.125	0.061	0.454	12.0408
0.13	0.065	0.371	11.0989
0.133	0.082	0.566	9.4036
0.139	0.111	0.642	7.1028
0.142	0.126	0.641	4.9713
0.146	0.121	0.681	6.4814
0.155	0.031	0.717	11.0726
0.174	0.022	0.636	10.1167
0.193	0.152	0.756	9.3023
0.077	0.042	0.465	13.5135
0.081	0.081	0.324	6.3424
0.097	0.045	0.451	9.2307
0.125	0.076	0.656	12.0408
0.13	0.045	0.787	11.9081
0.133	0.052	0.468	9.4036
0.139	0.091	0.636	7.1028
0.142	0.106	0.652	4.9713
0.146	0.071	0.611	6.4814
0.155	0.041	0.539	11.0726
0.174	0.082	0.716	10.1167

0.193	0.125	0.856	9.3023
0.077	0.112	0.495	13.5135
0.081	0.071	0.524	6.3424
0.097	0.095	0.651	9.23076
0.125	0.076	0.446	12.0408
0.13	0.035	0.675	11.0098
0.133	0.072	0.428	9.4034
0.139	0.161	0.736	7.1028
0.142	0.056	0.642	4.9713
0.146	0.111	0.451	6.4814
0.155	0.091	0.621	11.0726
0.174	0.102	0.536	10.1167
0.193	0.065	0.751	9.3023
0.077	0.032	0.856	13.513
0.081	0.101	0.441	6.3424
0.097	0.115	0.224	9.23076
0.125	0.106	0.660	12.0408
0.13	0.085	0.532	11.2112
0.133	0.062	0.712	9.4036
0.139	0.101	0.528	7.1028
0.142	0.103	0.717	4.9713
0.146	0.117	0.801	6.4814
0.155	0.091	0.398	11.0726
0.174	0.120	0.801	10.1167
0.193	0.125	0.856	9.3023
Average			**8.6389**

3.6 Conclusions

1- Eco-Friendly Synthesized was prepared of Copper oxide Nanoparticles using *Anchusa strigosa L.* Flowers .

2- Synthesized Copper oxide nanoparticles (CuO NPs) was characterized and confirmed by FT-IR , XRD ,and SEM techniques .

3- The synthesized particles were very stable, globular in shape with mean crystal size (28.22) nm.

4- The CuO NPs were applied for their adsorption activity to remove the basic Safranine dye from aqueous solution.

5- Removing of Gongo red from water was applied successfully by using synthesized CuO NPs which used as an adsorbent material.

6- The best efficiency of adsorption was gained by0.0300g adsorbent surface weight with 35 mg/L of Congo Red dye solutions at 30 minutes and pH (3).

7- The good conditions were perfect for safranine dye adsorption which was performed when0.0100g from that adsorbed particles with 20 minutes adsorption time and pH=9 and in 298 K.

8- Thermodynamic studies revealed that sorption of both dyes onto CuONPs were different . Change in enthalpy, ΔH, values obtained were(-23.1271) (Physisorption) for Congo red and (12.2731)(Chemisorption) for Safranin

9- The equilibrium information for adsorption has been outfitted to the Langmuir, Freundlich, Temkin and Halsey adsorption isotherm types.

10- The isothermal Freundlich and Halsey models gave a good linear relationship with the adsorption for Congo Red Safranin dyes using surface the CuONPs .

11- CuO nanoparticles did not cause hemolysis and therefore can be used in pharmaceutical fields .

12- It is preferable to use CuO NPs at low concentrations in hemolysis.

References

References

References

[1]   S. Bayda, M. Adeel, T. Tuccinardi, M. Cordani, and F. Rizzolio, "The history of nanoscience and nanotechnology: from chemical–physical applications to nanomedicine," *Molecules,* vol. 25, no. 1, p. 112, 2019.

[2]   G. A. Mansoori and T. F. Soelaiman, *Nanotechnology--An introduction for the standards community*. ASTM International, 2005.

[3]   S. Kargozar and M. Mozafari, "Nanotechnology and Nanomedicine: Start small, think big," *Materials Today: Proceedings,* vol. 5, no. 7, pp. 15492-15500, 2018.

[4]   V. Singh ,P. Yadav, and V. Mishra, "Recent advances on classification, properties, synthesis, and characterization of nanomaterials," *Green synthesis of nanomaterials for bioenergy applications,* pp. 83-97, 2020.

[5]   C. Buzea, I. Pacheco, and K. Robbie, "Nanoparticle classification," *Nanomaterials and nanoparticles: sources and toxicity. Biointerphases,* pp. 26-27, 2007.

[6]   A. H. Darwesh, S. B. Aziz, and S. A. Hussen, "Insights into optical band gap identification in polymer composite films based on PVA with enhanced optical properties: Structural and optical characteristics," *Optical Materials,* vol. 133, p. 113007, 2022.

[7]   N. Kumar and S. Kumbhat, *Essentials in nanoscience and nanotechnology*. John Wiley & Sons, 2016.

[8]   Z. Xue, C. Yan, and T. Wang, "From atoms to lives: The evolution of nanoparticle assemblies," *Advanced Functional Materials,* vol. 29, no. 12, p. 1807658, 2019.

[9]   T. Friscic, I. Huskic, S. Krivovichev, and I. Pekov, "Minerals with metal-organic framework structures," in *ACTA CRYSTALLOGRAPHICA A-FOUNDATION AND ADVANCES*, 2017, vol. 73, pp. C840-C840: INT UNION CRYSTALLOGRAPHY 2 ABBEY SQ, CHESTER, CH1 2HU, ENGLAND.

[10]   S. Pincebourde and H. A. Woods, "There is plenty of room at the bottom: microclimates drive insect vulnerability to climate change," *Current Opinion in Insect Science,* vol. 41, pp. 63-70, 2020.

[11]   C. N. R. Rao, A. Müller, and A. K. Cheetham, *The chemistry of nanomaterials: synthesis, properties and applications*. John Wiley & Sons, 2006.

[12]   S. Zhao *et al.*, "Ultrathin metal–organic framework nanosheets for electrocatalytic oxygen evolution," *Nature Energy,* vol. 1, no. 12, pp. 1-10, 2016.

[13]   H. Song, T. Kim, S. Kang, H. Jin, K. Lee, and H. J. Yoon, "Ga-Based liquid metal micro/nanoparticles: recent advances and applications," *Small,* vol. 16, no. 12, p. 1903391, 2020.

[14]   S. Iravani, "Green synthesis of metal nanoparticles using plants," *Green Chemistry,* vol. 13, no. 10, pp. 2638-2650, 2011.

[15]   M. J. Guajardo-Pacheco, J. Morales-Sánchez, J. González-Hernández, and F. Ruiz, "Synthesis of copper nanoparticles using soybeans as a chelant agent," *Materials letters,* vol. 64, no. 12, pp. 1361-1364, 2010.

[16]   Y. Xi *et al.*, "Morphology and phase selective synthesis of CuxO (x= 1, 2) nanostructures and their catalytic degradation activity," *Materials Science and Engineering: B,* vol. 166, no. 1, pp. 113-117, 2010.

[17]   R. Motoyoshi *et al.*, "Fabrication and characterization of cuprous oxide: fullerene solar cells," *Synthetic metals,* vol. 160, no. 11-12, pp. 1219-1222, 2010.

[18]   A. Khan, A. Rashid, R. Younas, and R. Chong, "A chemical reduction approach to the synthesis of copper nanoparticles," *International Nano Letters,* vol. 6, no. 1, pp. 21-26, 2016.

[19]   H. M. Fahmy, N. M. Ebrahim, and M. H. Gaber, "In-vitro evaluation of copper/copper oxide nanoparticles cytotoxicity and genotoxicity in normal and cancer lung cell lines," *Journal of Trace Elements in Medicine and Biology,* vol. 60, p. 126481, 2020.

References

[20] M. Nasrollahzadeh, M. Sajjadi, J. Dadashi, and H. Ghafuri, "Pd-based nanoparticles: Plant-assisted biosynthesis, characterization, mechanism, stability, catalytic and antimicrobial activities," *Advances in colloid and interface science,* vol. 276, p. 102103, 2020.

[21] M. E. Grigore, E. R. Biscu, A. M. Holban, M. C. Gestal, and A. M .Grumezescu, "Methods of synthesis, properties and biomedical applications of CuO nanoparticles," *Pharmaceuticals,* vol. 9, no. 4, p. 75, 2016.

[22] Z. Yan and D. B. Chrisey, "Pulsed laser ablation in liquid for micro-/nanostructure generation," *Journal of Photochemistry and Photobiology C: Photochemistry Reviews,* vol. 13, no. 3, pp. 204-223, 2012.

[23] H. Zeng *et al.*, "Nanomaterials via laser ablation/irradiation in liquid: a review," *Advanced Functional Materials,* vol. 22, no. 7, pp. 1333-1353, 2012.

[24] V. Amendola and M. Meneghetti, "What controls the composition and the structure of nanomaterials generated by laser ablation in liquid solution?," *Physical Chemistry Chemical Physics,* vol. 15, no. 9, pp. 3027-3046, 2013.

[25] M. S. Samuel, S. Jose, E .Selvarajan, T. Mathimani, and A. Pugazhendhi, "Biosynthesized silver nanoparticles using Bacillus amyloliquefaciens; Application for cytotoxicity effect on A549 cell line and photocatalytic degradation of p-nitrophenol," *Journal of Photochemistry and Photobiology B: Biology,* vol. 202, p. 111642, 2020.

[26] N. Ghasemi, F. Jamali-Sheini, and R. Zekavati, "CuO and Ag/CuO nanoparticles: Biosynthesis and antibacterial properties," *Materials Letters,* vol. 196, pp. 78-82, 2017.

[27] S. Saif Hasan *et al.*, "Bacterial synthesis of copper/copper oxide nanoparticles," *Journal of nanoscience and nanotechnology,* vol. 8, no. 6, pp. 3191-3196, 2008.

[28] S. C. Mali, S. Raj, and R. Trivedi, "Biosynthesis of copper oxide nanoparticles using Enicostemma axillare (Lam.) leaf extract," *Biochemistry and biophysics reports,* vol. 20, p. 100699, 2019.

[29] F. Duman, I. Ocsoy, and F. O. Kup, "Chamomile flower extract-directed CuO nanoparticle formation for its antioxidant and DNA cleavage properties," *Materials Science and Engineering: C,* vol. 60, pp. 333-338, 2016.

[30] R. Thapa, C. Bhagat, P. Shrestha, S. Awal, and P. Dudhagara, "Enzyme-mediated formulation of stable elliptical silver nanoparticles tested against clinical pathogens and MDR bacteria and development of antimicrobial surgical thread," *Annals of clinical microbiology and antimicrobials,* vol. 16, no. 1, pp. 1-10, 2017.

[31] H. Chakravarty, "Plant wealth of Iraq, Vol. I," *Ministry of Agriculture and Agrarian Reforms. Baghdad,* vol. 506, 1976.

[32] S. Dresler, G. Szymczak, and M. Wójcik, "Comparison of some secondary metabolite content in the seventeen species of the Boraginaceae family," *Pharmaceutical biology,* vol. 55, no. 1, pp. 691-695, 2017.

[33] S. A. Ghalib and E. J. Kadhim, "The Investigation of Some Phytochemical Compounds Found in Anchusa strigosa L. Grown Naturally in Iraq," *Iraqi Journal of Pharmaceutical Sciences (P-ISSN: 1683-3597, E-ISSN: 2521-3512),* vol. 30, no. 1, pp. 179-188, 2021.

[34] K. TABAN AKÇA, N. Eruygur, and O. Üstün, "Biological activity studies on the aqueous methanol extract of Anchusa undulata L. subsp. hybrida (Ten.) Coutinho," *Journal of Research in Pharmacy,* vol. 22, no. 3, 2018.

[35] D. Jakovljević, S. Vasić, M. Stanković, M. Topuzović, and L. Čomić, "The content of secondary metabolites and in vitro biological activity of Anchusa officinalis L.(Boraginaceae)," 2016.

[36] A. E. Al-Snafi, "Therapeutic properties of medicinal plants: a review of plants with antioxidant activity (part 1)," *International Journal of Pharmacology and Toxicology,* vol. 6, no. 3, pp. 159-182, 2015.

[37] M. Bacanlı, H. G. Göktaş, N. Başaran, N. Arı, and A. A. Başaran, "Beneficial effects of commonly used phytochemicals in diabetes mellitus," 2016.

References

[38] L. Tsalkovich, S. Sallon, H. Paavilainen, and H. Rosenmann" ,AntialzheimerLs disease related activities of Israeli medicinal plants," *JSM AlzheimerLs Disease and Related Dementia,* vol. 2, pp. 1015-1022, 2015.

[39] M. Abbas, A. Disi, and S. Al-Khalil, "Isolation and Identification of anti-ulcer components from Anchusa strigosa root," *Jordan J. Pharm. Sci,* vol. 2, no. 2, p. 131139, 2009.

[40] H. Zollinger, *Color chemistry: syntheses, properties, and applications of organic dyes and pigments*. John Wiley & Sons, 2003.

[41] A. Özcan, Ç. Ömeroğlu, Y. Erdoğan, and A. S .Özcan, "Modification of bentonite with a cationic surfactant: an adsorption study of textile dye Reactive Blue 19," *Journal of hazardous materials,* vol. 140, no. 1-2, pp. 173-179, 2007.

[42] S. Srinivasan *Chitra, K Balakameswari, K Sri Suthanthararajan, R Maheswari, B Uma Ravindranath, E Rajamani, S* "Decolourisation of leather dye by ozonation," *Desalination,* vol. 235, no. 1-3, pp. 88-92, 2009.

[43] A. Khenifi, Z. Bouberka, F. Sekrane, M. Kameche, and Z. Derriche, "Adsorption study of an industrial dye by an organic clay," *Adsorption,* vol. 13, no. 2, pp. 149-158, 2007.

[44] P. Gregory, "Classification of dyes by chemical structure," *The chemistry and application of dyes,* pp. 17-47, 1990.

[45] V. Vimonses, S. Lei, B. Jin, C. W. Chow, and C. Saint, "Kinetic study and equilibrium isotherm analysis of Congo Red adsorption by clay materials," *Chemical Engineering Journal,* vol. 148, no. 2-3, pp. 354-364, 2009.

[46] S. Taghavi Fardood, F. Moradnia, and A. Ramazani, "Green synthesis and characterisation of ZnMn2O4 nanoparticles for photocatalytic degradation of Congo red dye and kinetic study," *Micro & Nano Letters,* vol. 14, no. 9, pp. 986-991, 2019.

[47] V. Gupta, R. Jain, A. Mittal, M. Mathur, and S. Sikarwar, "Photochemical degradation of the hazardous dye Safranin-T using TiO2 catalyst," *Journal of colloid and interface science,* vol. 309, no. 2 ,pp. 464-469, 2007.

[48] L. Rosenberg, "Chemical basis for the histological use of safranin O in the study of articular cartilage," *JBJS,* vol. 53, no. 1, pp. 69-82, 1971.

[49] I. Ghosh, S. Kar, T. Chatterjee, N. Bar, and S. K. Das, "Adsorptive removal of Safranin-O dye from aqueous medium using coconut coir and its acid-treated forms: Adsorption study, scale-up design, MPR and GA-ANN modeling," *Sustainable Chemistry and Pharmacy,* vol. 19, p. 100374, 2021.

[50] G. K. Rajahmundry, C. Garlapati, P. S. Kumar ,R. S. Alwi, and D.-V. N. Vo, "Statistical analysis of adsorption isotherm models and its appropriate selection," *Chemosphere,* vol. 276, p. 130176, 2021.

[51] K. Czelej, K. Cwieka, and K. J. Kurzydlowski, "CO2 stability on the Ni low-index surfaces: van der Waals corrected DFT analysis," *Catalysis Communications,* vol. 80, pp. 33-38, 2016.

[52] G. Crini, "Non-conventional low-cost adsorbents for dye removal: a review," *Bioresource technology,* vol. 97, no. 9, pp. 1061-1085, 2006.

[53] A. S. Özcan, B. Erdem ,and A. Özcan, "Adsorption of Acid Blue 193 from aqueous solutions onto BTMA-bentonite," *Colloids and Surfaces A: Physicochemical and Engineering Aspects,* vol. 266, no. 1-3, pp. 73-81, 2005.

[54] B. Nandi, A. Goswami, and M. Purkait, "Removal of cationic dyes from aqueous solutions by kaolin: kinetic and equilibrium studies," *Applied Clay Science,* vol. 42, no. 3-4, pp. 583-590, 2009.

[55] V. Puccia and M. J. Avena, "On the use of the Dubinin-Radushkevich equation to distinguish between physical and chemical adsorption at the solid-water interface," *Colloid and Interface Science Communications,* vol. 41, p. 100376, 2021.

[56] R. Haddad *et al.*, "Journal of Iraqi Industrial Research," *Journal of Iraqi Industrial Research Vol,* vol. 2, no. 1, pp. 25-30, 2015.

References

[57]   K. Oura, M. Katayama, A. Zotov, V. Lifshits, and A. Saranin, "Atomic structure of surfaces with adsorbates," in *Surface Science*: Springer, 2003, pp. 195-227.

[58]   G. Z. Kadhim, "Astudy of Adsorption of some heavy metal on selected Iraqi Clay Surfaces ", University of Baghdad, 2010.

[59]   J. T. Richardson, V. Zhdanov, and L. Lloyd, "Fundamental and applied catalysis," ed: Springer, 1989.

[60]   C. Bellmann, "Surface modification by adsorption of polymers and surfactants," in *Polymer surfaces and interfaces* :Springer, 2008, pp. 235-259.

[61]   M. Xia *et al.*, "Removal of Hg (II) in aqueous solutions through physical and chemical adsorption principles," *RSC advances,* vol. 9, no. 36, pp. 20941-20953, 2019.

[62]   I. A. k. I. Gerasimov, *Physical chemistry*. Mir Publishers, 1974.

[63]   G. Tchobanoglous, F. L. Burton, and H. D. Stensel, "Wastewater engineering: treatment and reuse, Metcalf & Eddy Inc," *McGraw-Hill, Inc., New York. doi,* vol. 10, p. 0070418780, 2003.

[64]   I. M. Tawfeeq and A. J. Mohammed, "Adsorption Ability and Kinetic of (Congo Red, Methyl Green) Dyes on Iraqi Siliceous Rocks," 2009.

[65]   V. P. Ravi, R. V. Jasra, and T. S. Bhat, "Adsorption of phenol, cresol isomers and benzyl alcohol from aqueous solution on activated carbon at 278, 298 and 323 K," *Journal of Chemical Technology & Biotechnology: International Research in Process, Environmental AND Clean Technology,* vol. 71, no. 2, pp. 173-179, 1998.

[66]   D. A. Skoog, F. J. Holler, and S. R. Crouch, *Principles of instrumental analysis*. Cengage learning.2017 ,

[67]   R. Dandge, M. Ubale, M. Farooqui, and S. Rathod, "Adsorption study for the removal of hazardous dye Congo red by biowaste materials as adsorbents," *International Journal of Application or Innovation in Engineering & Management,* vol. 5, no. 11 ,pp. 9-16, 2016.

[68]   Q. Jiuhui, "Research progress of novel adsorption processes in water purification: a review," *Journal of environmental sciences,* vol. 20, no. 1, pp. 1-13, 2008.

[69]   R. APAK, G. ATUN, K. GUCLU, E. TUTEM, and G. KESKIN, "Colloid Chemistry Colloid Chemistry 200,207, 1978," *Journal of nuclear science and technology,* vol. 32, no. 10, pp. 1008-1017, 1995.

[70]   D. Barry and M. Cook, "Adsorption of cyclohexane and benzene on two modified silica supports," *The Journal of Physical Chemistry* ,vol. 79, no. 23, pp. 2555-2562, 1975.

[71]   J. A. Schramke, S. F. Murphy, W. J. Doucette, and W. D. Hintze, "Prediction of aqueous diffusion coefficients for organic compounds at 25 C," *Chemosphere,* vol. 38, no. 10, pp. 2381-2406, 1999.

[72]   G. M. Barrow ,*Physical chemistry for the life sciences*. McGraw-Hill College, 1981.

[73]   C. S. Goldenstein, R. M. Spearrin, J. B. Jeffries, and R. K. Hanson, "Infrared laser-absorption sensing for combustion gases," *Progress in Energy and Combustion Science,* vol. 60, pp. 132-176, 2017.

[74]   C. Giles, T. MacEwan, S. Nakhwa, and D. Smith, "786. Studies in adsorption. Part XI. A system of classification of solution adsorption isotherms, and its use in diagnosis of adsorption mechanisms and in measurement of specific surface areas of solids," *Journal of the Chemical Society (Resumed),* pp. 3973-3993, 1960.

[75]   I. Langmuir, "The adsorption of gases on plane surfaces of glass, mica and platinum," *Journal of the American Chemical society,* vol. 40, no. 9, pp. 1361-1403, 1918.

[76]   P. Atkins, P. W. Atkins, and J. de Paula, *Atkins' physical chemistry*. Oxford university press, 2014.

[77]   A. López, N. Lázaro, S. Morales, and A. M. Marqués, "Nickel biosorption by free and immobilized cells of Pseudomonas fluorescens 4F39: a comparative study," *Water, Air, and Soil Pollution,* vol. 135, no. 1, pp. 157-172, 2002.

[78]   R. Perry and C. Chilton, "Chemical Engineers' Handbook . New York: McGraw Hill," *Chemical Engineering Series,* 1973.

References

[79]	H. Freundlich, "Über die adsorption in lösungen ",*Zeitschrift für physikalische Chemie,* vol. 57, no. 1, pp. 385-470, 1907.

[80]	I. D. Mall, V. C. Srivastava, N. K. Agarwal, and I. M. Mishra, "Removal of congo red from aqueous solution by bagasse fly ash and activated carbon: kinetic study and equilibrium isotherm analyses," *Chemosphere,* vol. 61, no. 4, pp. 492-501, 2005.

[81]	M. Temkin and V. Pyzhev, "Recent modifications to Langmuir isotherms," 1940.

[82]	N. Ayawei, A. T. Ekubo, D. Wankasi, and E. D. Dikio, "Adsorption of congo red by Ni/Al-CO3: equilibrium, thermodynamic and kinetic studies," *Oriental Journal of Chemistry,* vol. 31, no. 3, p. 1307, 2015.

[83]	G. Halsey, "Physical adsorption on non-uniform surfaces," *The Journal of chemical physics,* vol. 16, no. 10, pp. 931-937, 1948.

[84]	M. Tarasev ,S. Chakraborty, K. Alfano, M. Muchnik, X. Gao, and R. Davenport, "Use of Packed Red Blood Cell Mechanical Fragility to Indicate Transfusion Outcomes," *medRxiv,* 2022.

[85]	S. Naz, A. Gul, and M. Zia, "Toxicity of copper oxide nanoparticles: a review study ",*IET nanobiotechnology,* vol. 14, no. 1, pp. 1-13, 2020.

[86]	C. Egbuna *et al.*, "Toxicity of nanoparticles in biomedical application: nanotoxicology," *Journal of Toxicology,* vol. 2021, 2021.

[87]	T. Ameh and C. M. Sayes, "The potential exposure and hazards of copper nanoparticles: A review," *Environmental Toxicology and Pharmacology,* vol. 71, p. 103220, 2019.

[88]	Z. Chen *et al.*, "Acute toxicological effects of copper nanoparticles in vivo," *Toxicology letters,* vol. 163, no. 2, pp. 109-120, 2006.

[89]	A .A. Motar, R. A. Hussein, and M. Abdulbary, "Study of in vitro and in vivo cytotoxicity effect of some medicinal plants | البيطرية الطبية للعلوم الكوفة مجلة ," *Kufa Journal For Veterinary Medical Sciences,* vol. 7, no. 2, 2016.

[90]	S. Kawanishi, S. Inoue, and K. Yamamoto, "Hydroxyl radical and singlet oxygen production and DNA damage induced by carcinogenic metal compounds and hydrogen peroxide," *Biological Trace Element Research,* vol. 21, no. 1, pp. 367-372, 1989.

[91]	L. M. Gaetke and C. K. Chow, "Copper toxicity, oxidative stress, and antioxidant nutrients," *Toxicology,* vol. 189, no. 1-2, pp. 147-163, 2003.

[92]	H. L. Karlsson, P. Cronholm, J. Gustafsson, and L. Moller, "Copper oxide nanoparticles are highly toxic: a comparison between metal oxide nanoparticles and carbon nanotubes," *Chemical research in toxicology,* vol. 21, no. 9, pp. 1726-1732, 2008.

[93]	A. M. Studer *et al.*, "Nanoparticle cytotoxicity depends on intracellular solubility: comparison of stabilized copper metal and degradable copper oxide nanoparticles," *Toxicology letters,* vol. 197, no. 3, pp. 169-174, 2010.

[94]	W.-S. Cho *et al.*, "Progressive severe lung injury by zinc oxide nanoparticles; the role of Zn2+ dissolution inside lysosomes," *Particle and fibre toxicology,* vol. 8, no. 1, pp.2011 ,16-1 .

[95]	P. Sutradhar, M. Saha, and D. Maiti, "Microwave synthesis of copper oxide nanoparticles using tea leaf and coffee powder extracts and its antibacterial activity," *Journal of Nanostructure in Chemistry,* vol. 4, no. 1, pp. 1-6, 2014.

[96]	R .Sivaraj, P. K. Rahman, P. Rajiv, H. A. Salam, and R. Venckatesh, "Biogenic copper oxide nanoparticles synthesis using Tabernaemontana divaricate leaf extract and its antibacterial activity against urinary tract pathogen," *Spectrochimica Acta Part A: Molecular and Biomolecular Spectroscopy,* vol. 133, pp. 178-181, 2014.

[97]	S. Singh, N. Kumar, M. Kumar, A. Agarwal, and B. Mizaikoff, "Electrochemical sensing and remediation of 4-nitrophenol using bio-synthesized copper oxide nanoparticles," *Chemical engineering journal,* vol. 313, pp. 283-292, 2017.

[98]	D. Devipriya and S. M. Roopan, "Cissus quadrangularis mediated ecofriendly synthesis of copper oxide nanoparticles and its antifungal studies against Aspergillus niger, Aspergillus flavus," *Materials Science and Engineering: C,* vol. 80, pp. 38-44, 2017.

References

[99]   M. Bordbar, Z. Sharifi-Zarchi, and B. Khodadadi, "Green synthesis of copper oxide nanoparticles/clinoptilolite using Rheum palmatum L. root extract: high catalytic activity for reduction of 4-nitro phenol, rhodamine B, and methylene blue," *Journal of sol-Gel science and Technology,* vol. 81, no. 3, pp. 724-733, 2017.

[100]   A. Kerour, S. Boudjadar, R. Bourzami, and B. Allouche, "Eco-friendly synthesis of cuprous oxide (Cu_2 O) nanoparticles and improvement of their solar photocatalytic activities," *Journal of Solid State Chemistry,* vol. 263, pp. 79-83, 2018.

[101]   Z. Vaseghi, O. Tavakoli, and A. Nematollahzadeh, "Rapid biosynthesis of novel Cu/Cr/Ni trimetallic oxide nanoparticles with antimicrobial activity," *Journal of Environmental Chemical Engineering,* vol. 6, no. 2, pp. 1898-1911, 2018.

[102]   E. Panneerselvam *et al.*, "Plant-Based Synthesis Processes for the Productionof Metal and Nonmetal Nanoparticles," in *Biological Synthesis of Nanoparticles and Their Applications*: CRC Press, 2019, pp. 47-64.

[103]   M. Gowri, N. Latha, and M. Rajan, "Copper oxide nanoparticles synthesized using Eupatorium odoratum, Acanthospermum hispidum leaf extracts, and its antibacterial effects against pathogens: a comparative study," *BioNanoScience,* vol. 9, no. 3, pp. 545-552, 2019.

[104]   P. Thakur and V. Kumar, "Kinetics and thermodynamic studies for removal of methylene blue dye by biosynthesize copper oxide nanoparticles and its antibacterial activity," *Journal of Environmental Health Science and Engineering,* vol. 17, no. 1, pp. 367-376, 2019.

[105]   S. Andra *et al.*, "Phytosynthesized metal oxide nanoparticles for pharmaceutical applications," *Naunyn-Schmiedeberg's archives of pharmacology,* vol. 392, no. 7, pp. 755-771, 2019.

[106]   J. E. Jeronsia, L. A. Joseph, P. A. Vinosha, A. J. Mary, and S. J. Das, "Camellia sinensis leaf extract mediated synthesis of copper oxide nanostructures for potential biomedical applications," *Materials Today: Proceedings,* vol. 8, pp. 214-222, 20.19

[107]   S. A. Akintelu, A. S. Folorunso, F. A. Folorunso, and A. K. Oyebamiji, "Green synthesis of copper oxide nanoparticles for biomedical application and environmental remediation," *Heliyon,* vol. 6, no. 7, p. e04508, 2020.

[108]   I. Karaj, "Raw and modified rice husk performance in removal of Basic Blue 41 from aqueous solutions," *Journal of Occupational and Environmental Health,* vol. 1, no. 1, pp. 41-49, 2016.

[109]   T. N. Chikwe, R. E. Ekpo, and I. Okoye, "Competitive adsorption of organic solvents using modified and unmodified calcium bentonite clay mineral," *Chem. Int,* vol. 4, no. 4, pp. 230-239, 2018.

[110]   A. K. Daylee, "Green Synthesis of Copper Nanoparticles Using Myrtus communis Leaves Extract: Characterization and Applications," University of Kerbala, 2022.

[111]   R. A. Hamouda, M. H. Hussein, R. A. Abo-Elmagd, and S. S. Bawazir, "Synthesis and biological characterization of silver nanoparticles derived from the cyanobacterium Oscillatoria limnetica," *Scientific reports,* vol. 9, no. 1, pp. 1-1.2019 ,7

[112]   M. Farrokhi, S.-C. Hosseini, J.-K. Yang, and M. Shirzad-Siboni, "Application of ZnO–Fe3O4 nanocomposite on the removal of azo dye from aqueous solutions: kinetics and equilibrium studies," *Water, Air, & Soil Pollution,* vol. 225, no. 9, pp.2014 ,12-1 .

[113]   P. Dey and R. Das, "Effect of silver doping on the elastic properties of CdS nanoparticles," *Indian Journal of Physics,* vol. 92, no. 9, pp. 1099-1108, 2018.

[114]   F. E. a. Meva *et al.*, "Silver and palladium nanoparticles produced using a plant extract as reducing agent, stabilized with an ionic liquid: sizing by X-ray powder diffraction and dynamic light scattering," *Journal of Materials Research and Technology,* vol. 8, no. 2, pp. 1991-2000, 2019.

[115]   M. Scimeca, S. Bischetti, H. K. Lamsira, R. Bonfiglio, and E. Bonanno, "Energy Dispersive X-ray (EDX) microanalysis: A powerful tool in biomedical research and diagnosis," *European journal of histochemistry: EJH,* vol. 62, no. 1, 2018.

References

[116] F. Adam, K. M. Hello, and H. Osman, "Synthesis of Mesoporous Silica Immobilized with 3-[(Mercapto or amino) propyl] trialkoxysilane by a Simple One-pot Reaction," *Chinese Journal of Chemistry,* vol. 28, no. 12, pp. 2383-2388, 2010.

[117] C. Akcay and M. Yalcin, "Morphological and chemical analysis of Hylotrupes bajulus (old house borer) larvae-damaged wood and its FTIR characterization," *Cellulose,* vol. 28, no. 3, pp. 1295-1310, 2021.

[118] T. J. Al-Hasani, H. H. Mihsen, K. M. Hello, and F. Adam, "Catalytic esterification via silica immobilized p-phenylenediamine and dithiooxamide solid catalysts," *Arabian Journal of Chemistry,* vol. 10, pp. S1492-S1500, 2017.

[119] O. M. Olabemiwo, A. Lateef, F. O. Agunbiade, S. Akanji, and H. O. Bakare, "The effects on oxidative aging, physical and flow properties of Agbabu natural bitumen modified with silver nanoparticles," *Heliyon,* vol. 6, no. 6, p. e04164, 2020.

[120] V. Gnanavel, V. Palanichamy, and S. M. Roopan, "Biosynthesis and characterization of copper oxide nanoparticles and its anticancer activity on human colon cancer cell lines (HCT-116)," *Journal of Photochemistry and Photobiology B: Biology,* vol. 171, pp. 133-138, 2017.

[121] R. Sankar, R. Maheswari, S. Karthik, K. S. Shivashangari, and V. Ravikumar, "Anticancer activity of Ficus religiosa engineered copper oxide nanoparticles," *Materials Science and Engineering: C,* vol. 44, pp. 234-239, 2014.

[122] A. A. Badawy, N. A. Abdelfattah, S. S. Salem, M. F. Awad, and A. Fouda, "Efficacy assessment of biosynthesized copper oxide nanoparticles (CuO-NPs) on stored grain insects and their impacts on morphological and physiological traits of wheat (Triticum aestivum L.) plant," *Biology,* vol. 10, no. 3, p. 233, 2021.

[123] V. Ramadhan, Y. Ni'mah, E. Yanuar, and S. Suprapto, "Synthesis of copper nanoparticles using Ocimum tenuiflorum leaf extract as capping Agent," in *AIP Conference Proceedings*, 2019, vol. 2202, no. 1, p. 020067: AIP Publishing LLC.

[124] N. Sebeia, M. Jabli, and A. Ghith, "Biological synthesis of copper nanoparticles, using Nerium oleander leaves extract: characterization and study of their interaction with organic dyes," *Inorganic Chemistry Communications,* vol. 105, pp. 36-46, 2019.

[125] B. Varghese, M. Kurian, S. Krishna, and T. Athira, "Biochemical synthesis of copper nanoparticles using Zingiber officinalis and Curcuma longa: Characterization and antibacterial activity study," *Materials Today: Proceedings,* vol. 25, pp. 302-306, 2020.

[126] M. Rafique *Muhammad Shaikh, Ahson J Rasheed, Reena Tahir, Muhammad Bilal Bakhat, Hafiz Faiq Rafique, Muhammad Shahid Rabbani, Faiz*, "A review on synthesis, characterization and applications of copper nanoparticles using green method," *Nano,* vol. 12, no. 04, p. 1750043, 2017.

[127] A. Bhatnagar, A. Jain, V. Gupta, S. Jain, and S. Suhas, "A comparative assessment of adsorbents prepared from industrial wastes for the removal of cationic dye," *Journal of the Indian Chemical Society,* vol. 80, pp. 267-270, 2003.

[128] M. K. Uddin, S. S. Ahmed, and M. Naushad, "A mini update on fluoride adsorption from aqueous medium using clay materials," *Desalination and Water Treatment,* vol. 145, pp. 232-248, 2019.

[129] A. M. Abbas, Y. I .Mohammed, and T. A. Himdan, "Adsorption kinetic and thermodynamic study of congo red dye on synthetic zeolite and modified synthetic zeolite," *Ibn AL-Haitham Journal For Pure and Applied Science,* vol. 28, no. 1, pp. 54-72, 2017.

[130] M. L. F. A. De Castro, M. L. B. Abad, D. A. G. Sumalinog, R. R. M. Abarca, P. Paoprasert, and M. D. G. de Luna, "Adsorption of methylene blue dye and Cu (II) ions on EDTA-modified bentonite: isotherm, kinetic and thermodynamic studies," *Sustainable Environment Research,* vol ,28 .no. 5, pp. 197-205, 2018.

[131] V. P. Vinod and T. S. Anirudhan, "Sorption of tannic acid on zirconium pillared clay," *Journal of Chemical Technology & Biotechnology: International Research in Process, Environmental & Clean Technology,* vol. 77, no. 1 ,pp. 92-101, 2002.

References

[132]   F. Elmi, F. Mohammadi Damghani, and M. Shokrollahzadeh Taleshi, "Kinetic and isotherm studies of adsorption of the metribuzin herbicide on an Fe3O4/CNT@ PDA hybrid magnetic nanocomposite in wastewater," *Industrial & Engineering Chemistry Research,* vol. 59, no. 20, pp. 9604-9610, 2020.

[133]   P. Saha and S. Chowdhury, "Insight into adsorption thermodynamics," *Thermodynamics,* vol. 16, pp. 349-364, 2011.

[134]   A. M. Aljeboree, N. Abd Alrazzak, M. B. Alqaraguly, M. A. Mahdi, L. S. Jasim, and A. F. Alkaim, "Adsorption of pollutants by using low-cost (Environment-Friendly): Equilibrium, kinetics and thermodynamic studies: A review," *Systematic Reviews in Pharmacy,* vol. 11, no. 12, pp. 1988-1997, 2020.

[135]   M. Zohra and A. Fawzia, "Hemolytic activity of different herbal extracts used in Algeria," *Int J Pharm Sci Res,* vol. 5, no. 8, pp. 495-500, 2014.

[136]   M. Gondwal and G. Joshi nee Pant, "Synthesis and catalytic and biological activities of silver and copper nanoparticles using Cassia occidentalis," *International Journal of Biomaterials,* vol. 2018, 2018.

[137]   B. M. Rothen-Rutishauser, S. Schürch, B. Haenni, N. Kapp, and P. Gehr, "Interaction of fine particles and nanoparticles with red blood cells visualized with advanced microscopic techniques," *Environmental science & technology,* vol. 40, no. 14, pp. 4353-4359, 2006.

<u>الخلاصة</u>

في هذه الدراسة ، تم استخدام طريقة خضراء فعالة رخيصة التكلفة لتخليق جزيئات أوكسيد النحاس النانوية (CuO NPs) باستخدام المستخلص المائي لزهرة لسان الثور في درجة حرارة الغرفة. شخصت جزيئات أوكسيد النحاس المُصنَّعة بواسطة التحليل الطيفي للأشعة فوق البنفسجية المرئية (UV-VIS)، والتحليل الطيفي للأشعة تحت الحمراء (FTIR)، والفحص المجهري الإلكتروني (SEM) ، وتحليل الأشعة السينية المشتتة للطاقة (EDX-Elemental) وتقنية حيود الأشعة السينية (XRD) . وظهرت الجسيمات المصنعة مستقرة جدًا ، كروية الشكل معدل الحجم البلوري (28.22) نانومتر. تم اختبار جزيئات أوكسيد النحاس النانوية لأمتزاز أصباغ الكونغو الحمراء والسفرانين من محاليلها المائي. ودراسة العوامل المؤثر على ازالة الصبغتين باستخدام دقائق اوكسيد النحاس النانوية مثل زمن الاتزان، وزن السطح الماز ،الدالة الحامضية ، تأثير الشدة الأيونية وتأثير درجة الحرارة (الايزوثيرمات) وتم فحص بيانات العملية بواسطة موديلات الامتزاز لانكماير ,فرندلش , تمكن و هلسي عند درجات حرارة مختلفة (318-288 كلفن) وقد تم حساب قيم الدوال الثرم ديناميكية وهي (ΔG   ΔH, ΔS,) وقد تم حسابها لعملية امتزاز أصباغ الكونغو الحمراء والسفرانين على جزيئات أوكسيد النحاس النانوية عند درجات حرارة مختلفة (318-288 كلفن) ان التغير في قيم الانثالبي والتي كانت (23.1271-) وهذا يعني باعث للحراره بالنسبة لصبغة الكونغو الحمراء وذا يدل على ان التفاعل امتزاز فيزيائي (12.2731) وهذا يعني ماص للحراره بالنسبة لصبغة السفرانين وهذا يدل على ان التفاعل امتزاز كيميائي . ان موديلات امتزاز فرندلش وهلسي اعطت افضل علاقة خطية مع امتزاز صبغتي الكونغو الحمراء والسفرانين بأستخدام جزيئات النحاس النانوية. ظهر شكل الايزوثيرم لكلا الصبغتين يأخذ شكل حرف S4 طبقا لتصنيف جيلز. تمت دراسة التوافق الدموي لجزيئات أوكسيد النحاس النانوية عن طريق اختبارات انحلال الدم باستخدام كريات الدم الحمراء البشرية المأخوذة من متطوعين أصحاء عدد 60 .

التخليق الأخضر لجزيئات أوكسيد النحاس النانوية ودراسة تأثيرها على إزالة الصبغات وتحلل الدم.

رسالة مقدمة الى

مجلس كلية العلوم – جامعة كربلاء

كجزء من استكمال متطلبات نيل درجة الماجستير

علوم في الكيمياء

من قبل

صفاء علي كحيط موسى الكريطي

اشراف

أ. د . أيمان طالب كريم

أ. م.د . أحسان مهدي شهيد

2023 م

1445 هــ